Endocrinology, 2021, Vol. 162, No. 4, 1–22
doi:10.1210/endocr/bqab024
Research Article

Research Article

Osteogenic Mechanisms of Basal Ganglia Calcification and its ex vivo Model in the Hypoparathyroid Milieu

Parmita Kar,[1] Tabin Millo,[2] Soma Saha,[1] Samrina Mahtab,[1] Shipra Agarwal,[3] and Ravinder Goswami[1]

[1]Department of Endocrinology and Metabolism, All India Institute of Medical Sciences, New Delhi 110029, Delhi, India; [2]Department of Forensic Medicine and Toxicology, New Delhi 110029, Delhi, India; and [3]Department of Pathology, All India Institute of Medical Sciences, New Delhi 110029, Delhi, India

ORCiD number: 0000-0002-3097-5074 (R. Goswami).

Abbreviations: β-GP, β-glycerophopshate; ALP, alkaline phosphatase; BGC, basal ganglia calcification; CA-II, carbonic anhydrase-II; CNPase, 2′,3′ cyclic nucleotide 3′-phosphodiesterase; DAPI, 4′,6-diamidino-2-phenylindole; DMEM, Dulbecco's modified Eagle's medium; ENPP1, ectonucleotide pyrophosphatase family member 1; FBS, fetal bovine serum; FGFR, fibroblast growth factor receptor; FTIR, Fourier-transform infrared spectroscopy; GFAP, glial fibrillary acidic protein; $hPTH_{(1-34)}$, human recombinant parathyroid hormone; IPG, immobilized pH gradient gel; ISG15, interferon-stimulated gene-15; LRP5, low-density lipoprotein receptor–related protein 5; MGP, Matrix GLA protein; mRNA, messenger RNA; Msx-2, Msx-homebox-2; NeuN, neuronal nuclei; NT_5E, ecto-5′-nucleotidase; OPG, osteoprotegerin; PBS, phosphate-buffered saline; PCDH12, protocadherin 12; PCR, polymerase chain reaction; PDGF, platelet-derived growth factor; PDGFR-β, platelet-derived growth factor-receptor-β; PFA, paraformaldehyde; PTH, parathyroid hormone; PTHR2, parathyroid hormone–receptor 2; RANK, receptor activator of nuclear factor kappa B; RANK-L, ligand of the receptor activator of nuclear factor kappa B; RIN, RNA integrity number; RT, reverse-transcriptase; SDS-PAGE, sodium dodecyl sulfate–polyacrylamide gel electrophoresis; SOX2, sex-determining region Y box 2; TIP39, tuberoinfundibular peptide of 39 residues; USP18, ubiquitin-specific peptidase 18; Wnt, wingless related integration site; XPR1, xenotropic and polytropic retrovirus receptor 1

Received: 8 September 2020; Editorial Decision: 29 January 2021; First Published Online: 4 February 2021; Corrected and Typeset: 5 March 2021.

Abstract

Context: Basal-ganglia calcification (BGC) is common (70%) in patients with chronic hypoparathyroidism. Interestingly, cortical gray matter is spared from calcification. The mechanism of BGC, role of hyperphosphatemia, and modulation of osteogenic molecules by parathyroid hormone (PTH) in its pathogenesis is not clear.

Objective: We assessed the expression of a large repertoire of molecules with proosteogenic or antiosteogenic effects, including neuroprogenitor cells in caudate, dentate, and cortical gray matter from normal autopsy tissues. The effect of high phosphate and PTH was assessed in an ex vivo model of BGC using striatum tissue culture of the Sprague-Dawley rat.

Methods: The messenger RNA and protein expression of 39 molecules involved in multiple osteogenic pathways were assessed in 25 autopsy tissues using reverse-transcriptase polymerase chain reaction, Western blot, and immunofluorescence. The striatal culture was maintained in a hypoparathyroid milieu for 24 days with and without

ISSN Online 1945-7170

(a) high phosphate (10-mm β-glycerophosphate) and (b) $PTH_{(1-34)}$ (50 ng/mL Dulbecco's modified Eagle's medium–F12 media) for their effect on striatal calcification and osteogenic molecules.

Results: Procalcification molecules (osteonectin, β-catenin, klotho, *FZD4*, *NT_5E*, *LRP5*, *WNT3A*, collagen-1α, and *SOX2*-positive neuroprogenitor stem cells) had significantly higher expression in the caudate than gray matter. Caudate nuclei also had higher expression of antiosteogenic molecules (osteopontin, carbonic anhydrase-II [*CA-II*], *MGP*, sclerostin, *ISG15*, *ENPP1*, and *USP18*). In an ex vivo model, striatum culture showed an increased propensity for calcified nodules with mineral deposition similar to that of bone tissue on Fourier-transformed infrared spectroscopy, alizarin, and von Kossa stain. Mineralization in striatal culture was enhanced by high phosphate and decreased by exogenous PTH through increased expression of *CA-II*.

Conclusion: This study provides a conceptual advance on the molecular mechanisms of BGC and the possibility of PTH therapy to prevent this complication in a hypoparathyroid milieu.

Key Words: hypoparathyroidism, basal ganglia calcification, hyperphosphatemia, ex vivo model, osteogenic molecules

Intracranial calcifications are observed in up to 70% of patients with chronic hypoparathyroidism (1, 2). The basal ganglia, cerebellum, and its dentate nuclei are the most common sites. Interestingly, cortical gray matter is usually spared from such calcification (2). Our previous clinical studies in patients with hypoparathyroidism revealed an association of basal ganglia calcification (BGC) with hyperphosphatemia and several neuropsychiatric symptoms, including Parkinsonism and chorea (3). The mechanism of predilection of basal ganglia for calcification and the direct effect of parathyroid hormone (PTH) on this calcification is not clear. The lack of availability of striatum tissue (caudate and putamen nuclei) from patients with hypoparathyroidism is a major limitation to studying the mechanism of BGC. Earlier in 2014, we first assessed a set of 16 osteogenic molecules modulating bone mineralization and observed a high expression of osteopontin and carbonic anhydrase-II (*CA-II*) in the caudate nuclei of individuals with normal findings (4).

The present study assessed a large repertoire of additional molecules involved in multiple aspects of calcification in the caudate, dentate, and cortical gray matter obtained from autopsies of individuals with normal findings. We also developed an ex vivo culture model to understand the interplay of various molecules in the development of BGC in hypoparathyroidism. These molecules cover pathways related to bone morphogenesis, Wnt-signaling, matrix glycoproteins, phosphate transporters, osteogenic differentiation, PTH-receptor 2 (PTHR2) and its ligand, markers of stem cells, and molecules related to familial BGC (5, 6). The ex vivo tissue culture model of BGC was developed using rat striatum following observation of similarity in its expression of osteogenic molecules akin to human caudate nucleus. The model was used to investigate the ability of human recombinant parathyroid hormone, $hPTH_{(1-34)}$ to inhibit BGC and its effect on striatal and brain-specific adenyl-cyclase and other osteogenic molecules.

Material and Methods

Osteogenic molecules with procalcification and anticalcification effects were assessed in caudate, dentate, and cortical gray tissues obtained from autopsies carried out at the Department of Forensic Medicine at the All India Institute of Medical Sciences, Delhi. The tissues were collected from those autopsies, which were performed within 12 hours of death (n = 39) following approval of the institutional ethics committee, and consent from the relatives of the deceased (IECPG-50/16.02.17). None of the deceased had a history suggestive of hypoparathyroidism. The dissection of the caudate and cortical gray matter was described in detail in our earlier study (4). The dentate nucleus was separated at its serrated margin from the sagittal section of the cerebellum lobes (Fig. 1A). All the tissues were quickly transported on ice to the endocrine laboratory and stored in multiple aliquots in liquid nitrogen. A portion of each tissue was processed for paraffin sectioning to confirm the histology of the caudate by pencil fibers and the dentate nucleus by its principal small circuit neurons using 0.1% cresyl violet stain. All experiments including RNA extraction, complementary DNA preparation, and reverse-transcriptase polymerase chain reaction (RT-PCR) were carried out within 2 months of tissue collection. The details of osteogenic molecules assessed, their messenger

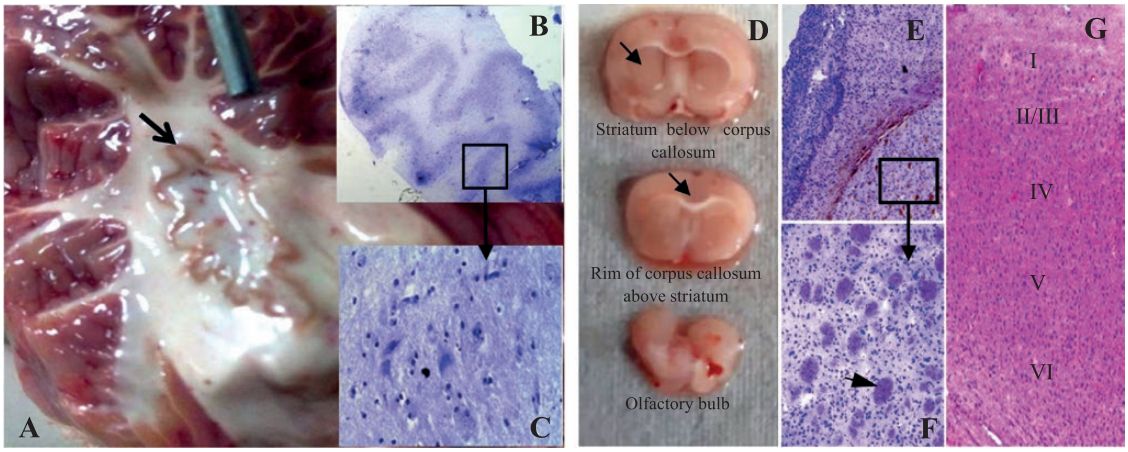

Figure 1. Dissection of the dentate nucleus from the autopsies and striatum tissue from Sprague-Dawley rat brain. A, Sagittal section of the cerebellum lobe showing dentate nucleus with serrated margins. B, Paraffin section stained with 0.1% cresyl violet at 20× magnification showing distinct serrated margins of dentate and C, oval principal and small circuit neurons at 400× magnification. D, Ventral olfactory bulb and 2 sequential coronal sections of the rat brain showing corpus striatum below the corpus callosum (arrow), and E, 0.05% Toludine blue–stained paraffin section of coronal sections of rat brain showing striatum and gray tissue at 400×. F, Striatum showing Wilson's pencils at 1000× (arrow). G, Hematoxylin-eosin stain of the cortical gray matter showing organization into six layers in the gray matter (400×).

RNA (mRNA) and protein expression analysis, confocal microscopy for localization in different types of brain cells, and the development of the ex vivo culture model are given below.

Osteogenic Molecules and Their Primers

The mRNA expression analysis was carried out by RT-PCR for molecules known to have a vital role in osteogenesis. In addition, we included molecules that showed a remarkable difference in the expression on RNA microarray in paired human caudate and cortical gray tissues from 4 autopsies. Briefly, we studied mRNA expression of Dickkopf-1, receptor activator of nuclear factor kappa B (*RANK*) and its ligand (*RANK-L*), and osteoprotegerin (OPG) involved in bone remodeling and morphogenesis (7). Other molecules included were the matrix glycoproteins GLA protein (*MGP*), fetuin, Msx-homebox-2 (*Msx-2*), and ectonucleotide pyrophosphatase family member 1 (*ENPP1*); Klotho, fibroblast growth factor receptor 1 and 4 (*FGFR1*, *FGFR4*) as markers of osteogenesis; wingless related integration site (*WNT*) *3A* and *WNT5*, ecto-*5′*-nucleotidase (NT_5E), receptor and members of Wnt pathway such as frizzled 4 and 9 (*FZD 4* and *9*), β-catenin, and low-density lipoprotein receptor–related protein *5* (*LRP5*); bone-specific alkaline phosphatase (*ALP*) and collagen 1-α were assessed as markers of osteoblastic activity, and tuberoinfundibular peptide of 39 residues (*TIP39*), a ligand of *PTHR2*, and chordin as bone morphogenic antagonist (8-14). Molecules linked with familial BGC were also assessed, including interferon-stimulated gene-15 (*ISG15*), xenotropic and polytropic retrovirus receptor 1 (*XPR1*), ubiquitin-specific peptidase 18 (USP18), platelet-derived growth factor (*PDGF*), and protocadherin 12 (*PCDH12*). Expression of pleuripotent stem cell was assessed by sex-determining region Y box 2 (*SOX2*) and neuroectodermal stem cell (Nestin) markers. Neural-progenitor, mesenchymal stem cells, and brain-specific pericytes were identified by expression of *CD133*, *CD90*, and platelet-derived growth factor-receptor-β (*PDGFR*-β), respectively (15, 16). The present study also reassessed the expression of osteonectin, osteopontin, *CA-II*, *PTHR2*, and phosphate transporter (Pit 1 and 2), which were found to be significant in our previous study (4). Overall, 19 of these molecules had known procalcification action in bone mineral homeostasis (*WNT3*A and *WNT5*, *FZD4* and *FZD9*, β-catenin, *LRP5*, collagen-1α, *ALP*, *Msx-2*, osteonectin, NT_5E, klotho, *TIP39*, fetuin, osteoprotegerin, *FGFR1* and *FGFR4*, and *Pit1* and *Pit2*). Fifteen molecules assessed had anticalcification action (*CA-II*, osteopontin, sclerostin, dickkopf1, *RANK* and *RANKL*, *MGP*, *ENPP1*, chordin, *ISG15*, *USP18*, *XPR1*, *PCDH12*, *PDGF*, and *PTHR2*) (4, 6-8, 13, 14, 17-22). The primers used for mRNA expression are shown in Supplementary Table 1 (23).

Reverse-Transcriptase Polymerase Chain Reaction and RNA microarray

Total RNA from autopsy tissues was extracted using a RNA binding column (Pure Link RNA Mini Kit, Thermo Fisher Scientific) and quantified by an ultraviolet spectrophotometer (GeneQuant; Amersham). RNA integrity (RIN) was checked using an eukaryotic total RNA

6000 Nano kit on a Bioanalyzer 2100 machine (Agilent Technologies). Only those tissues for which RIN was greater than 7.0 were included in this study (24). Random hexamers were used to prepare complementary DNA, and RT-PCR was performed using Brilliant III SYBR (Agilent) on a CFX96 thermocycler (Bio-Rad GmbH) as described earlier (4). The mRNA expression of a test molecule in caudate, gray matter, and dentate tissues from each autopsy was assayed in duplicates and in the same plate to minimize assay variation. The conditions for PCR and size of amplicon are shown in Supplementary Table 1 (23). The specificity of amplified products following RT-PCR was checked by 2% agarose electrophoresis and DNA sequencing (25). The mRNA expression was normalized using the geometric mean of cytochrome-C1 (*CYC1*), hypoxanthine phosphoribosyl transferase, and tyrosine-monooxygenase expression. These housekeeping genes were selected based on their good score for stable expression in Ge-Norm analysis (26).

RNA microarray analysis was carried out using complementary RNA prepared from 100 ng of total RNA, labeled with cyanine3′-CTP and hybridized on Human SurePrint G3 Human GE 8 × 60k microarray chips (Agilent). The chip was read using a microarray scanner and analyzed using GeneSpring 13.0 software. Osteogenic molecules with more than a 4-fold difference in expression between the caudate and gray matter were considered significant and included for RT-PCR in all 25 autopsy samples.

Western Blot Analysis and 2-Dimensional Electrophoresis

A total of 40 mg each of caudate, dentate, and gray matter tissues were lysed in radioimmunoprecipitation assay buffer by sonication, and 50 µg of protein from each lysates were loaded in wells for sodium dodecyl sulfate (SDS)–polyacrylamide gel electrophoresis (PAGE) (6%-10%). Protein expression of various osteogenic molecules was assessed by Western blot on a deca-probe manifold using specific antibodies (27). Proteins that could not be detected by Western blot after 1-dimension electrophoresis were further analyzed by 2-dimensional (2D) electrophoresis using 12-cm immobilized pH gradient gel (IPG) strips (pH 3-10, Agilent). Briefly, lysates for loading on IPG strips were prepared by sonicating 40-mg tissue each from caudate, dentate, and gray matter in 500 µL of 10% w/v lysis buffer (8 M urea, 2 M thiourea, and 1% SDS). The protein in the lysates was precipitated by methanol chloroform (3:1), redissolved in 2D buffer (Agilent), and quantified using Qubit 4 Fluorometer (Thermo Fisher Scientific). A total of 500 µg of protein from different tissues was loaded onto multiwell IPG strips and run at 1500 V to separate proteins in 12 fractions using off-gel isoelectric point focusing. The fractions were selected according to the isoelectric pH of osteogenic molecules, and 50 µg from each of the 12 fractions were loaded on SDS-PAGE for 2D separation and Western blot. In all the blots, ALP-labeled secondary antibodies were used. BCIP/NBT (VWR Chemicals) was used for color development. The sources of various antibodies and dilution used are shown in Supplementary Table 2 (23).

Localization of Osteogenic Proteins in Different Brain Cells

Localization of osteogenic proteins in neurons, astrocytes, oligodendrocytes, and endothelial cells was assessed by indirect immunofluorescence (IIF). Briefly, 4 sections (10 µm) each from caudate, dentate, and gray matter were used for each osteogenic molecule. Following antigen retrieval in a decloaking chamber (Biocare Medical), all 12 sections were incubated with primary antibodies (1:250 dilution each, against a test osteogenic molecule and a brain cell marker). The brain cell markers used were antineuronal nuclei (NeuN) for neurons, glial fibrillary acidic protein (GFAP) for astrocytes, 2′,3′ cyclic nucleotide 3′- phosphodiesterase (CNPase) for oligodendrocytes, and CD31 for endothelial cells. Sections were counterstained with secondary antibodies (1:500 dilution each, antirabbit Alexa Fluor 488 for osteogenic molecules and antimouse Alexa Fluor 546 for brain cell markers, Thermo Fisher Scientific) and DAPI (4′,6-diamidino-2-phenylindole; Sigma Aldrich) for nuclear localization. Images were acquired using an inverted confocal microscope (FV10-ASW 1.7, Olympus). Anti-Nestin, CD133, CD90, and PDGFR-β antibodies were used to localize different types of stem cells in each section.

Ex Vivo Model of Basal Ganglia Calcification

The ex vivo model was developed using striatum tissue from adult Sprague-Dawley rats (~ 220 g each) procured from the central animal facility. All the experiments were conducted after institutional animal ethics committee approval (92/IAEC-1/2018) as per the guidelines of the Committee for the Purpose of Control and Supervision of Experiments on Animals (28). The rats were euthanized in a CO_2 chamber and striatum tissue was dissected as described by Spijker (29). Briefly, the skull bone was opened at its junction with the nasal bone and the whole brain was removed en bloc with the cerebellum and washed with ice-cold phosphate-buffered saline (PBS). The olfactory bulb was removed and 2 sequential coronal sections were cut at 2.0-mm intervals to reach the striatum region, which was indicated by a rim of white corpus callosum above it (Fig. 1D). The striatum and the cortical gray matter were dissected clear from the corpus callosum. Pencil fibers on histology and

high mRNA expression of the *Darpp32* molecule were checked in the removed tissue to confirm its identity as striatum (Fig. 1E-1G). The expression of various osteogenic molecules modulating bone mineralization in the striatum and its gray matter was assessed by RT-PCR in 6 rats using sequence-specific primers (Supplementary Table 3) (23). The mRNA expression was normalized by *Cyc1*, *β-actin*, and *18s-rRNA* genes (30). The specificity of amplicons was checked by 2% agarose electrophoresis (Supplementary Figure 1) (23).

Primary Cell Culture of Rat Striatum and Cortical Gray Tissue

The striatum and cortical gray tissues were put in cold Dulbecco's modified Eagle's medium (DMEM)-F12 culture media containing 10% fetal bovine serum (FBS), 1-mmol L-glutamine, penicillin-streptomycin, normocin, and nonessential amino acids (Gibco, Invitrogen). Tissues were washed with ice-cold Hanks' balanced salt solution, minced, and centrifuged using 10-mL media at 400*g* for 5 minutes. Both tissues were separately dispersed in 10 mL of 0.1% Trypsin-Versene at 37 °C for 1 hour. Trypsin from the dispersed cells was neutralized by 10% FBS and cell suspension was pelleted at 400*g* for 5 minutes. Cell pellets were dispersed in culture media and seeded in poly-D-lysine–coated 6-well plates or on coverslips and incubated in humidified 95% air and 5% CO_2 at 37 °C. The growth of cells during the initial 5 days was facilitated by adding 10 ng/mL each of recombinant FGF and epidermal growth factors (Gibco).

Induction of Calcification in Striatum Cell Culture Under a Hypoparathyroid Milieu

The total calcium (1.33 mmol, 5.3 mg/dL) and phosphorus (1.29 mmol, 4.0 mg/dL) content of the DMEM-F12 media with 10% FBS resembled a low serum, low calcium but normal phosphorus milieu in human tissue. The hypocalcemic and hyperphosphatemic milieu of hypoparathyroidism was mimicked in cell culture by adding 10 mmol β-glycerophosphate (β-GP) to increase the phosphorus content of the DMEM-F12 media. Cells were cultured in β-GP containing media from day 6 to day 24 to induce calcification. Ascorbic acid (50 µg/mL) and dexamethasone (10 nM) were also added to the culture media to facilitate collagen synthesis (31). The experiments were repeated 3 times in separate rats.

Biochemical and Cellular Characterization of Calcification in Striatum Culture

The presence of nodules in the cell culture and their calcium and phosphorus deposits were assessed the 24th day by Alizarin Red-S and von Kossa stains (Sigma). Briefly, cells were washed with PBS, fixed with 4% paraformaldehyde (PFA), and incubated with 2% alizarin (pH 4.3) for 45 minutes (32). Excess stain was rinsed with deionized water and PBS. The area under alizarin stain was quantified as $pixel^2$ by the multiple image alignment tool using cellSens Dimension 2.1 software (Olympus, Japan). For von Kossa staining, cells were fixed in ice-cold 70% ethanol for 30 minutes and incubated with 5% silver nitrate for 45 minutes in an ultraviolet crosslinker at 1200 W (Amersham) and rinsed with deionized water. The hydroxyapatite content of calcium and phosphate deposits was assessed by Fourier-transform infrared spectroscopy (FTIR) in cells scraped from culture wells (33). These cells were desiccated in a speed-vac (Eppendorf) for 3 hours, powdered, mixed with potassium-bromide in a 1:100 ratio, and compressed hydraulically into a 13-mm disc. FTIR spectrum was obtained from 4000 to 400 λ at 4-λ intervals on an RXI spectrometer (PerkinElmer). Commercially obtained hydroxyapatite powder (Merck India Ltd) was used as a standard. A chip of human calvarial cortical bone obtained from autopsy was desiccated and finely powdered, and was used as an additional standard.

The cellular phenotype of the striatal cell culture was assessed day 5 of the culture and again on day 24 using cells grown on coverslips. These experiments were repeated twice in 2 rats with controls, including striatum cell culture from the same rats in media with no β-GP. Cells were fixed with 4% PFA and stained with anti-NeuN, GFAP, CNPase, CD31, and CD133 antibodies to identify different types of brain cells and neural-progenitor stem cells (15, 34). The presence of collagen and ALP in the nodules was assessed by staining with anticollagen-1α antibodies and BCIP/NBT, and the specific stain for each was quantified using cellSens software. The mineral deposit on the collagen matrix was assessed by scanning electron microscopy (EVO-50, Carl-Zeiss) after coating with 100-Å gold particles. To quantify change in cellular phenotype and extracellular matrix, RT-PCR was carried out to assess mRNA expression of *Fox3* coding for NeuN, *Gfap*, *Cnpase*, *Cd31*, *Cd133*, collagen-1α, and *Alp* .

Effect of Human Recombinant Parathyroid Hormone on Striatal Cell Calcification and Modulation of Osteogenic Molecules

$hPTH_{(1\text{-}34)}$ (Millipore) was added to the culture (50-ng/mL media) from day 6 onward to assess its effect on calcification. Media was replaced every 48 hours with fresh $hPTH_{(1\text{-}34)}$ each time for 24 days. These experiments were repeated 3 times in different rats and the striatal cell culture from the same rat without any added $hPTH_{(1\text{-}34)}$ served as a control. An MTT assay (5.0 mg/mL,

3-(4,5-dimethyl-2-thiazolyl)-2,5-diphenyl-2H-tetrazolium bromide; Sigma) was carried out in triplicate, each from 2 rats, to assess the effect of $hPTH_{(1-34)}$ exposure on cell viability with absorbance measured at 560 nm (iMark plate reader, Bio Rad). Striatal cell culture was carried out in another set of 6 rats to assess the modulatory effect of $hPTH_{(1-34)}$ on mRNA expression of various osteogenic molecules. However, these cells were cultured without β-GP and only for 16 days because of difficulty in extracting RNA on the 24th day from striatal cell culture showing calcified nodules. Expression of 5 isoforms of adenyl-cyclase was also assessed to determine an $hPTH_{(1-34)}$-specific effect (35–37).

Proportion of Different Cells in Striatum and Cortical Tissue, on Day 5 of Culture and After Addition of Parathyroid Hormone

The identity and proportion of various cells in the rat striatum and cortical tissues were determined using cell marker–specific antibodies against *NeuN*, *GFAP*, and *CNPase* by Accuri C6 flow cytometer (BD). Briefly, after dissection striatum and cortical tissues were minced and dispersed mechanically by repeated trituration with 1.0-mL pipette tips followed by incubation with Accutase enzyme (BD) for 30 minutes. Cells were sieved through 100- and 40-µm filters to obtain single-cell suspension for flowcytometry as described by Rubio et al (38). The dispersed cells were fixed in 4% PFA for 30 minutes and permeabilized using a Fix/Perm kit (eBiosciences). These cells were incubated with primary antibodies (1:50 dilution) for 1 hour and secondary antibodies (1:500) Alexa Fluor 647 (for GFAP), and Alexa Fluor 488 (for NeuN, CNPase) for 30 minutes on ice. Cells were analyzed at a flow rate of 14 µL/min and the percentages of different cells were determined using BD Accuri C6 software. The experiments were repeated 3 times in different rats with each experiment including unstained cells and cells stained with only secondary antibodies, that is, Alexa Fluor 488 and 647 of the same rats as controls. The same procedure was used to identify the proportion of different cells from striatum and cortical tissue culture on the fifth day and their change after PTH treatment.

Statistical Analysis

The mRNA copies of molecules expressed in caudate and gray matter in autopsies and in rat tissues are shown as mean ± SD, median, and interquartile range. The Shapiro-Wilk test was used to check for the normalcy of distribution of the distribution of mRNA. Log transformation of mRNA expression was performed for molecules with asymmetrical distribution. Log-transformed data were again checked for normalcy of the distribution, and a paired-sample *t* test was performed to assess the differences in mRNA expression. The area under alizarin stain in striatal cell culture is shown as mean ±SEM. The change in mRNA expression of various molecules in the rat striatal culture after PTH exposure is shown as fold change over an untreated sample using the Wilcoxon signed-rank test. *P* less than .05 was considered significant for all tests. The *P* values for molecules showing significant differences in expression were further corrected by multiplying by the number of molecules tested.

Results

Caudate and gray matter tissues were dissected in all 39 autopsies and dentate nuclei separated in 34 of them. Sufficient RNA was extracted from the caudate and gray matter in 33 cases (27 male, 6 female, mean age 34 ± 12 years). The causes of sudden death in these 33 individuals were road accident or cardiac arrest (n = 11 each), electrocution, cerebral stroke, and fall from height (3 each), stabbing, and gunshot injury (1 each). RNA with good RIN values (> 7.0) were extracted from the paired caudate and gray matter (8.9 ± 0.7 and 8.7 ± 1.0, *P* = .41) from 25 autopsies. The RIN was greater than 7 (7.7 ± 0.4) in only 11 of the 25 dentate tissues removed.

Messenger RNA Expression of Osteogenic Molecules in Human Autopsy Tissues

Fig. 2 shows the agarose gel electrophoresis of amplified products of all the osteogenic molecules after RT-PCR. These included *WNT-5*, collagen-1α, and chordin identified through RNA microarray with more than a 4-fold difference in the expression between caudate and gray matter (8.4-, 9.5-, and 9.7-fold, respectively). The mean mRNA expression of all molecules assessed in the 25 autopsies in the caudate and gray matter is shown in Table 1. Altogether, 20 molecules showed a significant difference between the caudate and gray matter even after stringent correction of *P* values. Among the proosteogenic molecules, osteonectin, β-catenin, klotho, *FZD4*, *NT$_5$E*, *LRP5*, *WNT3A*, and collagen-1α showed a significantly higher expression in the caudate than gray matter arranged in order of their mRNA copies. The first 4 of these molecules (β-catenin, osteonectin, klotho, and *FZD4*) had maximum differences in expression between the caudate and gray matter.

Among the antiosteogenic molecules, osteopontin, *CA-II*, *MGP*, sclerostin, *ISG15*, *ENPP1*, and *USP18* showed a significantly higher expression in caudate than gray arranged according to their mRNA copies. The difference in mRNA copies between the caudate and gray matter also followed the order shown earlier. Chordin, *RANK*, Dickkopf-1, and *PTHR2* had lesser expression in the caudate than the gray matter. Among various neuroprogenitor markers, *SOX2* showed a significantly higher expression in the caudate than the gray matter.

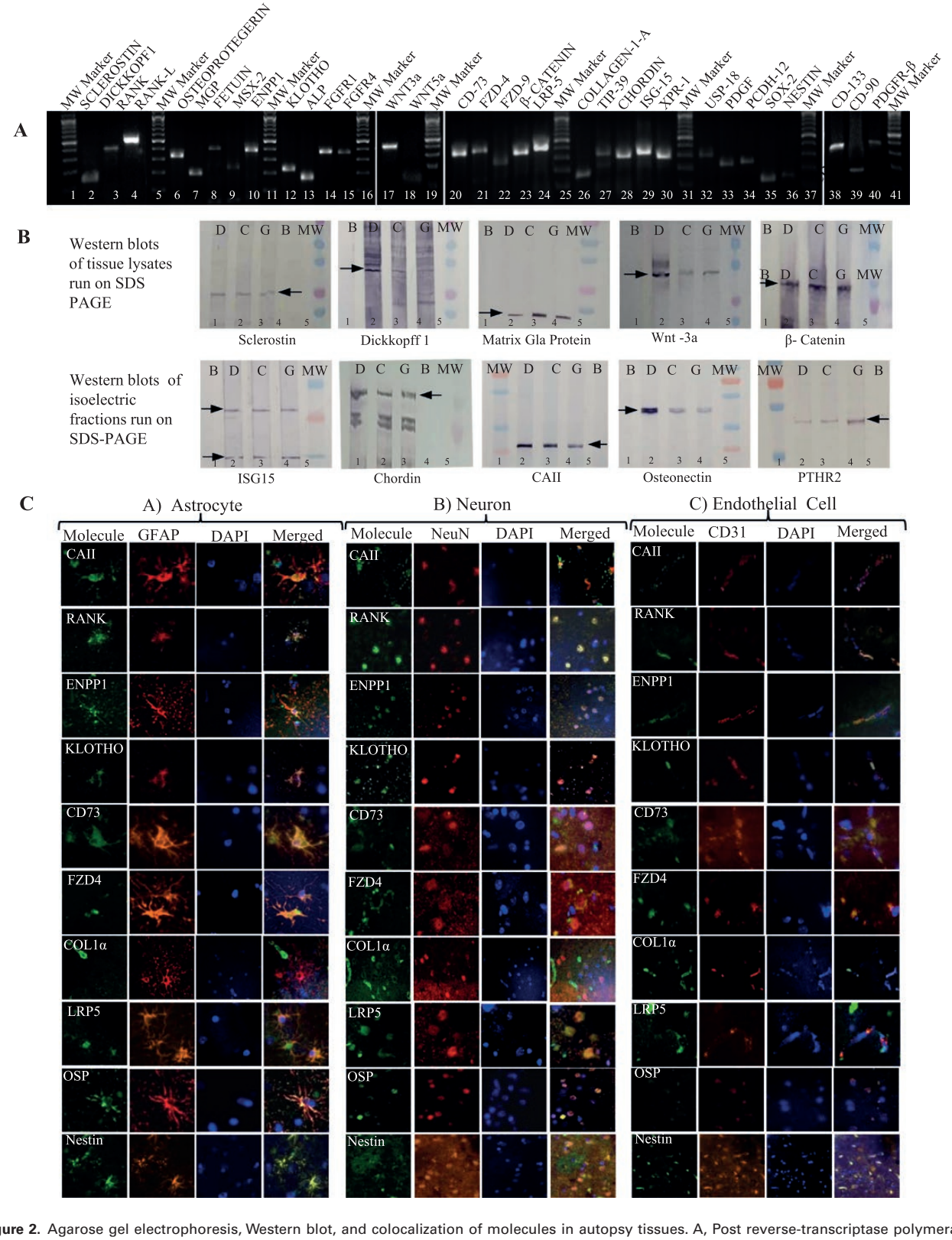

Figure 2. Agarose gel electrophoresis, Western blot, and colocalization of molecules in autopsy tissues. A, Post reverse-transcriptase polymerase chain reaction (PCR) 2% agarose gel electrophoresis of amplified products. B, Western blot in dentate, caudate, and gray tissues. C, Confocal microscopy images (600×) for localization of protein molecules along with brain cell markers NeuN, GFAP, and CD31. All osteogenic markers are labeled with AF488 (green), brain cell markers labeled with AF546 (red) and nucleus is stained with DAPI (blue). All 3 are merged to show co-localization. C, caudate; D, dentate; DAPI, 4′,6-diamidino-2-phenylindole; G, gray matter; GFAP, glial fibrillary acidic protein; MW, molecular-weight marker; NeuN, antineuronal nuclei.

Table 1. Messenger RNA copy numbers of study molecules in caudate and gray matter

SN	Gene	No.	mRNA/10^4 copies of housekeeping genes tested		Differences of copy (caudate to gray) Median (IQR)	*P*	*P*[a]
			Caudate	Gray			
Proosteogenic molecules							
1	β-Catenin						
	Mean ± SD	25	88 671 ± 139 923	31 836 ± 19 294	15 720 (2392 to 42 948)	< .001	.007
	Median (IQR)		48 775 (24 932-91 626)	27 955 (14 547-41 771)			
2	Osteonectin						
	Mean ± SD	25	248 417 ± 415 417	33 875 ± 27 639	9128 (22 825 to 148 872)	< .001	< .001
	Median (IQR)		117 436 (40 247-172 285)	24 849(14 495-44 988)			
3	Klotho						
	Mean ± SD	24	10 541 ± 9509	856 ± 965	7200 (2942 to 13 812)	< .001	< .001
	Median (IQR)		7587 (3071-17 113)	536 (190-1213)			
4	*FZD4*						
	Mean ± SD	21	15 208 ± 27 833	4066 ± 5535	1659 (209 to13746)	< .001	< .001
	Median (IQR)		3464 (429-19 019)	1346 (182-6672)			
5	*NT_5E*						
	Mean ± SD	23	4035 ± 6287	704 ± 828	1418 (581 to 1850)	< .001	< .001
	Median (IQR)		1680 (1096-2387)	433 (300-716)			
6	*LRP5*						
	Mean ± SD	23	4978 ± 8133	1002 ± 666	1115 (307 to 2522)	< .001	< .001
	Median (IQR)		2259 (8754-3164)	889 (592-1137)			
7	*WNT3A*						
	Mean ± SD	23	1253 ± 3020	177 ± 233	228 (13 to 511)	< .001	< .001
	Median (IQR)		323 (25-857)	59 (10-274)			
8	Collagen-1α						
	Mean ± SD	20	1946 ± 4677	93 ± 158	188 (77 to 1194)	< .001	< .001
	Median (IQR)		241 (139-1223)	14 (9-92)			
9	*WNT5A*						
	Mean ± SD	19	1351 ± 2012	728 ± 692	–26 (–164 to 370)	.97	NS
	Median (IQR)		272 (166-1825)	457 (311-670)			
10	*FZD9*						
	Mean ± SD	21	604 ± 934	117 ± 86	103 (6 to 259)	.003	NS
	Median (IQR)		160 (79-447)	96 (50-131)			
11	*ALP*						
	Mean ± SD	23	8333 ± 17 639	3784 ± 2674	187 (–1171 to 1323)	.30	NS
	Median (IQR)		2954 (1759–5418)	2711 (2039-4106)			
12	*MSX-2*						
	Mean ± SD	19	3076 ± 5403	1012 ± 927	404 (–115 to 1985)	.04	NS
	Median (IQR)		1045 (388-36 570)	806 (317-1437)			
13	*TIP39*						
	Mean ± SD	18	55 ± 108	14 ± 23	4.5 (–0.5 to 15.7)	.12	NS
	Median (IQR)		14 (1.4-37.4)	6.4(1.4-17.7)			
14	Fetuin						
	Mean ± SD	18	1658 ± 1663	1197 ± 1114	–24 (–421 to 1557)	.91	NS
	Median (IQR)		1183 (243-2622)	1014 (291-1489)			
15	Osteoprotegerin						
	Mean ± SD	25	2918 ± 8480	444 ± 586	111(–58 to 655)	.04	NS
	Median (IQR)		263 (117-1376)	217 (97-484)			
16	*FGFR1*						
	Mean ± SD	24	1852 ± 2684	905 ± 819	142 (–206 to 803)	.57	NS
	Median (IQR)		583 (227-2480)	473 (348-1818)			
17	*FGFR4*						
	Mean ± SD	23	567 ± 1318	96 ± 75	149 (5 to 284)	< .001	0.05
	Median (IQR)		208 (60-422)	73 (28-179)			
18	*PIT1*						
	Mean ± SD	25	5468 ± 5069	6375 ± 5291	–1187 (–5927 to 512)	.33	NS
	Median (IQR)		3633 (1670-9747)	4332 (2558-9777)			
19	*PIT2*						
	Mean ± SD	23	4166 ± 4271	2954 ± 1595	225 (–764 to 723)	.35	NS
	Median (IQR)		2223 (1858-4754)	2612 (1727-4149)			
Antiosteogenic molecules							
20	Osteopontin						
	Mean ± SD	24	772 771 ± 2 595 911	137 218 ± 434 747	71 317 (44 131 to 103 283)	< .001	< .001
	Median (IQR)		94 877 (73 583-200 478)	26 055(13 185-33 697)			
21	*CA-II*						
	Mean ± SD	24	47 098 ± 54 850	5249 ± 3406	11 726 (5974 to 79 140)	< .001	< .001
	Median (IQR)		16 411(9302–86 979)	4747 (2386-7867)			

Table 1. Continued

SN	Gene	No.	mRNA/10^4 copies of housekeeping genes tested		Differences of copy (caudate to gray) Median (IQR)	*P*	*P*[a]
			Caudate	Gray			
22	*MGP*						
	Mean ± SD	25	18 241 ± 24 726	3622 ± 2554	5168 (573 to 25 390)	< .001	.02
	Median (IQR)		7187(2905-29 783)	2766 (1768-5592)			
23	Sclerostin						
	Mean ± SD	23	7976 ± 15 882	1556 ± 2718	1286 (219 to 5650)	< .001	< .001
	Median (IQR)		2606 (391-6805)	527 (141-1448)			
24	*ISG15*						
	Mean ± SD	23	3059 ± 3434	1136 ± 1104	1135 (128 to 1912)	< .001	.007
	Median (IQR)		1884 (1105-3434)	802 (504-1503)			
25	*ENPP1*						
	Mean ± SD	23	1184 ± 1798	307 ± 175	240 (54 to 785)	< .001	.03
	Median (IQR)		477 (336-1091)	240 (187-433)			
26	*USP18*						
	Mean ± SD	23	374 ± 449	118 ± 92	93 (52 to 231)	< .001	.002
	Median (IQR)		222 (104-417)	96 (51-192)			
27	Chordin						
	Mean ± SD	19	3130 ± 8530	4975 ± 4511	–1809 (–4819 to –661)	< .001	.002
	Median (IQR)		573 (190-2136)	2935 (1905-7918)			
28	*RANK*						
	Mean ± SD	23	942 ± 2664	1082 ± 2120	–218 (–455 to –108)	< .001	.005
	Median (IQR)		118 (60-366)	403 (236-838)			
29	Dickkopf1						
	Mean ± SD	23	139 ± 193	200 ± 202	–55 (–104 to –2.5)	.001	.04
	Median (IQR)		92 (19-118)	126 (65-271)			
30	*PTHR2*						
	Mean ± SD	24	620 ± 1194	1161 ± 675	–546 (–1374 to –225)	< .001	.004
	Median (IQR)		159 (55-463)	1272 (539-1576)			
31	*RANKL*						
	Mean ± SD	18	4038 ± 7449	1767 ± 2609	–5.6 (–492 to 2177)	.99	NS
	Median (IQR)		405 (59-4030)	724 (76-2118)			
32	*XPR1*						
	Mean ± SD	23	8907 ± 8730	5733 ± 3475	1988 (–1273 to 5036)	.07	NS
	Median (IQR)		7460 (4230-9444)	5139 (3008-8313)			
33	*PCDH 12*						
	Mean ± SD	22	180 ± 290	35 ± 44	47 (–5 to 127)	.10	NS
	Median (IQR)		72 (19-142)	25 (13-36)			
34	*PDGF*						
	Mean ± SD	19	204 ± 273	73 ± 92	28 (–6 to 218)	.13	NS
	Median (IQR)		71 (22-340)	28(16-127)			
Stem cell markers							
35	*SOX2*						
	Mean ± SD	20	514 669 ± 766 202	111 200 ± 111 476	80 676 (24 965 to 235 165)	< .001	.02
	Median (IQR)		156 467 (91 103-333 546)	67 017(42 909-154 698)			
36	Nestin						
	Mean ± SD	18	1057 ± 2985	253 ± 269	105 (46 to 333)	.009	.34
	Median (IQR)		267 (149-570)	139 (78-318)			
37	*CD133*						
	Mean ± SD	14	32 ± 57	32 ± 59	4.6 (–18 to 13)	.44	NS
	Median (IQR)		13 (3-20)	3.0 (1.5-29.0)			
38	*CD90*						
	Mean ± SD	15	28 ± 57	10 ± 14	2.2 (–1.8 to 17)	.92	NS
	Median (IQR)		11(3–30)	5.9 (3.1-13.3)			
39	*PDGFR-β*						
	Mean ± SD	12	6.0 ± 8.1	1.3 ± 1.4	2.0 (0.2 to 4.4)	.06	NS
	Median (IQR)		2.7 (1.1-7.8)	1.0 (0.2-2.1)			

Abbreviations: *CA-II*, carbonic-anhydrase-II; *ENPP1*, ectonucleotide pyrophosphatase family member 1; *FGFR*, fibroblast growth factor receptor; IQR, interquartile range; *ISG15*, interferon stimulated gene-15; *LRP5*, lipoprotein receptor–related protein 5; *MGP*, GLA protein; mRNA, messenger RNA; *Msx-2*, Msx-homebox-2; *Nestin*, neuroectodermal stem cell; NS, not significant; *NT_5E*, ecto-5′-nucleotidase; *PDGF*, platelet-derived growth factor; *PDGFR-β*, platelet-derived growth factor receptor-β; *PTHR2*, parathyroid receptor 2; *RANK*, receptor activator of nuclear factor kappa B; *SOX2*, sex-determining region Y box 2; *TIP39*, tuberoinfundibular peptide of 39 residues; *USP18*, ubiquitin-specific peptidase 18; *XPR1*, xenotropic and polytropic retrovirus receptor 1.

[a]Corrected *P* value equals the *P* value multiplied by the total number of molecules tested: 39.

The pattern of mRNA expression of procalcification molecules (osteonectin, *FZD4*, *LRP5*, and *WNT3A*) and antiosteogenic molecules (osteopontin, *CA-II*, *MGP*, sclerostin, *ISG15*, *ENPP1*, and *USP18*, $P < .05$) in the dentate nucleus vs gray matter showed a trend similar to that of caudate (uncorrected $P < .05$ for all the molecules shown earlier, Table 2). However, the significance for several of these molecules was reduced following correction for number of values tested because of limited sample size.

Western Blot Analysis of Osteogenic Molecules

Western blot analysis of sclerostin, Dickkopf-1, MGP, Wnt-3a, β-catenin, chordin, ISG15, CAII, osteonectin, and PTHR2 showed visible expression in caudate, gray matter, and dentate tissues (Fig. 2B). Chordin, ISG15, CA-II, osteonectin, and PTHR2 required isoelectric focusing and 2D electrophoresis for visualization. Molecules that could not be identified on Western blot were detected by indirect immunofluorescence as discussed in the following section.

Localization of Osteogenic Proteins in Various Cells of Caudate, Gray Matter, and Dentate

In the caudate nucleus, all the osteogenic molecules were expressed in the neurons, endothelial cells, and astrocytes, except sclerostin, FZD4, and collagen-1α, which showed no expression in astrocytes (Fig. 2C). Similarly, in gray matter, most osteogenic molecules were expressed in neurons, astrocytes, and endothelial cells except sclerostin, FZD4, collagen-1α, ISG15, osteonectin, and PTHR2, which showed no expression in astrocytes. Klotho, FZD4, and PTHR2 could not be localized in endothelial cells of the cortical gray matter. Expression of most osteogenic molecules was poor or noninterpretable in the oligodendrocytes except for sclerostin, ENPP1, klotho, CA-II, and osteopontin (Supplementary Figure 2) (23). Nestin was expressed in neurons, astrocytes, and endothelial cells, and PDGFR-β was expressed in neurons and astrocytes both of the caudate and gray matter. CD133 was present both in the neuron and endothelial cells of the caudate tissue but was expressed only in the neurons of the cortical gray matter.

Ex Vivo Model of Basal Ganglia Calcification in Hypoparathyroidism

The striatal tissue dissected from rat brain showed pencil fiber–shaped corticostriatal tracts and higher mRNA expression of *Darpp-32* than the gray matter (Table 3). The pattern of mRNA expression assessed for 15 osteogenic molecules in striatum and gray matter in the rat was similar to that observed in corresponding human autopsy tissues. In fact, the difference in the expression of *Enpp1*, klotho, *Isg15*, osteopontin, *Pit1* and 2, collagen-1α, and *Ca-II* attained statistical significance despite a limited number of rats (n = 6).

Rat Striatum Tissue Culture and Development of Calcification

Striatal cell culture in the presence of β-GP showed multiple nodules on the 24th day of culture (Fig. 3). These nodules stained positive with alizarin and von Kossa and showed the presence of dense collagen fibrils. In contrast, the culture of the gray matter showed no remarkable calcification with and without β-GP. The size and number of nodules increased following the addition of β-GP–supplemented media in the striatum culture from 2 of the 3 rats. In the remaining 1 of the 3 rats, the area under alizarin stain was remarkably high and showed further change after the addition of β-GP. Fig. 3 shows the average increase of area under alizarin stain (1.8 ± 0.4-fold) following β-GP in rat striatal cell culture. Overall there was a 5.5 ± 1.2-fold difference in the area under alizarin stain between the striatal and cortical gray cell culture after the addition of β-GP. The FTIR analysis of the calcified nodules scraped from the culture wells showed an absorption spectrum that resembled peaks of calcium hydroxyapatite and human calvarial cortical bone (see Fig. 3).

Fig. 4 shows the effect of high phosphate on the modulation of the cellular phenotype and extracellular matrix in rat striatum cells on the 24th day of culture compared to the fifth day, before the addition of β-GP. The presence of phosphate increased extracellular collagen-1α secretion and ALP stain by an average of 11.8- and 9.3-fold respectively, respectively. Interestingly, β-GP led to a reduction in cells stained for neuron, astrocyte, oligodendrocytes, and endothelial cell markers with a concomitant increase in CD133-positive cells.

The mRNA expression of collagen-1α and *Cd133* significantly increased and *Cd31* significantly decreased following the procalcification media (Supplementary Table 4) (23). The expression of *Alp* tended to be 3-fold higher but did not reach statistical significance. The mRNA expression of *Gfap*, NeuN, and *Cnpase* was variable in different rats after the addition of the procalcification media.

Effect of Human Recombinant Parathyroid Hormone on Striatal Cell Culture Calcification and Osteogenic Molecules

The mean calcified area in the striatal cell culture determined by alizarin stain was reduced by 47% ($P = .002$) after $hPTH_{(1-34)}$ exposure compared to the untreated striatal cell culture from the same set of 3 rats (Fig. 5). Cell viability before and after $hPTH_{(1-34)}$ exposure showed no remarkable difference (92 ± 7% and 106 ± 20%, respectively). Table 4 summarizes the effect of $hPTH_{(1-34)}$ exposure on the mRNA expression of various molecules in striatal cell culture. The expression of *Nt5e, Wnt5a Fgfr1, Usp18, Ca-II*, and its signaling molecule Adenyl-cyclase 5 and 10 isoforms increased significantly after $hPTH_{(1-34)}$ exposure.

Table 2. mRNA expression of osteogenic molecules in dentate and gray matter

SN	Gene	mRNA/10^4copies of housekeeping genes		Difference of copies (dentate to gray)Median IQR	No.	*P*	*P*[a]
		Dentate	Gray				
Proosteogenic molecules							
1	β-Catenin						
	Mean ± SD	58 738 ± 51 207	43 802 ± 30 365	15 897 (–15 389 to 42 041)	8	.32	NS
	Median (IQR)	42 255 (29 158-63 879)	40 417 (15 919-69 630)				
2	Osteonectin						
	Mean ± SD	210 556 ± 134 622	25 855 ± 19 938	153 886 (59 311 to 318 983)	9	< .001	0.006
	Median (IQR)	179 326 (92 743-34 289)	25 440 (12 544-29 103)				
3	Klotho						
	Mean ± SD	526 ± 573	522 ± 683	20 (–422 to 826)	8	.84	NS
	Median (IQR)	233 (149-1081)	232 (117-651)				
4	*FZD4*						
	Mean ± SD	1403 ± 1102	3751 ± 390	1148 (167 to 1897)	7	.03	NS
	Median (IQR)	1183 (358-2315)	183 (157-537)				
5	*NT_5E*						
	Mean ± SD	685 ± 659	858 ± 882	–25 (–501 to 423)	9	.61	NS
	Median (IQR)	449 (198-1059)	478 (216-1428)				
6	*LRP5*						
	Mean ± SD	1812 ± 778	852 ± 393	910 (238 to 1712)	8	.008	NS
	Median (IQR)	1739 (1118-2414)	899 (560-991)				
7	*WNT3A*						
	Mean ± SD	50 ± 41	19 ± 19	23 (15 to 61)	9	.007	NS
	Median (IQR)	32 (23-75)	10 (5-32)				
8	*WNT5A*						
	Mean ± SD	1729 ± 1569	729 ± 428	308 (–143 to 2489)	5	.33	NS
	Median (IQR)	1100 (467-3306)	792 (147-1112)				
9	*FZD9*						
	Mean ± SD	212 ± 109	97 ± 68	126 (20 to 197)	6	.03	NS
	Median (IQR)	214 (100-329)	74 (47-147)				
10	*ALP*						
	Mean ± SD	2983 ± 806	2554 ± 1309	98 (–517 to 1540)	7	.37	NS
	Median (IQR)	2987 (2138-3964)	2459 (1656-2711)				
11	*MSX-2*						
	Mean ± SD	1213 ± 1321	481 ± 502	310 (50 to 1881)	8	.05	NS
	Median (IQR)	681 (387–2172)	266 (123–933)				
12	Osteoprotegerin						
	Mean ± SD	943 ± 1472	530 ± 792	220 (10 to 602)	9	.04	NS
	Median (IQR)	507 (265-786)	235 (83-725)				
13	*FGFR1*						
	Mean ± SD	2666 ± 5233	381 ± 198	432 (–272 to 3787)	6	.40	NS
	Median (IQR)	710 (237-4002)	416 (180-567)				
14	*FGFR4*						
	Mean ± SD	796 ± 587	189 ± 102	370 (198 to 1107)	7	.005	NS
	Median (IQR)	565 (339-1476)	194 (86-249)				
15	*PIT1*						
	Mean ± SD	19 782 ± 27 187	4742 ± 5053	2914 (1089 to 30 271)	9	.03	NS-
	Median (IQR)	5819 (3946-38 898)	2720 (1486-6555)				
16	*PIT2*						
	Mean ± SD	14 578 ± 20 828	3681 ± 2094	7131 (–388 to 8021)	8	.04	NS
	Median (IQR)	8943 (4176-11 051)	3167 (2290-4883)				

Table 2. Continued

SN	Gene	mRNA/10^4copies of housekeeping genes		Difference of copies (dentate to gray)Median IQR	No.	*P*	*P*[a]
		Dentate	Gray				
Antiosteogenic molecules							
17	Osteopontin						
	Mean ± SD	857 226 ± 464 407	24 262 ± 15 985	652 516 (494 811 to 1 262 978)	9	< .001	< .001
	Median (IQR)	666 152 (509 454-1 279 866)	21 635 (10 644-32 743)				
18	*CA-II*						
	Mean ± SD	112 091 ± 114 289	8000 ± 3256	78 972 (31 220 to 122 529)	8	< .001	.003
	Median (IQR)	84 088 (36 035–13 382)	7330 (4864-11 293)				
19	*MGP*						
	Mean ± SD	20 167 ± 19 954	4382 ± 4611	8106 (3607 to 29 872)	9	.006	NS
	Median (IQR)	10 821 (8522-33 854)	2280 (1768-5582)				
20	Sclerostin						
	Mean ± SD	1095 ± 665	228 ± 160	576 (464 to 1429)	9	< .001	< .001
	Median (IQR)	689 (628-1626)	178 (125-336)				
21	*ISG15*						
	Mean ± SD	6227 ± 6614	950 ± 578	2727 (1811 to 6987)	8	.003	NS
	Median (IQR)	4131 (2531-8159)	696 (506-1466)				
22	*ENPP1*						
	Mean ± SD	1923 ± 1348	250 ± 146	2143 (349 to 2492)	7	< .001	0.002
	Median (IQR)	2538 (537-2945)	205 (148-395)				
23	*USP18*						
	Mean ± SD	162 ± 140	84 ± 68	38 (9 to 116)	8	.05	NS
	Median (IQR)	112 (47-290)	58 (35-156)				
24	*RANK*						
	Mean ± SD	395 ± 710	326 ± 113	–172 (–285 to 341)	8	.08	NS
	Median (IQR)	70 (25-655)	317 (239-399)				
25	Dickkopf1						
	Mean ± SD	288 ± 271	118 ± 84	92 (–11 to 286)	9	.07	NS
	Median (IQR)	233 (91–424)	94 (48–182)				
26	*PTHR2*						
	Mean ± SD	54 ± 46	1018 ± 570	–863 (–1468 to –513)	8	< .001	.001
	Median (IQR)	40 (19-75)	903 (532-1547)				
27	*XPR1*						
	Mean ± SD	8793 ± 8577	4664 ± 3054	283 (–1240 to 10 222)	9	.04	NS
	Median (IQR)	6876 (2500-15 711)	3808 (2359-7226)				
28	*PCDH 12*						
	Mean ± SD	93 ± 83	32 ± 22	29 (9 to 115)	6	.02	NS
	Median (IQR)	45 (40-176)	30 (13-45)				
29	*PDGF*						
	Mean ± SD	73 ± 69	83 ± 138	9 (–18 to 38)	7	.63	NS
	Median (IQR)	31 (19-124)	27 (14-81)				

RANKL, fetuin, Collagen-1α, *TIP39*, and chordin were not tested because of the limitation of RNA extracted from dentate tissue.
[a]Corrected *P* value equals the *P* value multiplied by the total number of molecules tested: 29.

Proportion of Different Cells in Striatum and Cortical Tissue on Day 5 of Culture and After Addition of Parathyroid Hormone

The proportions of NeuN-, GFAP-, and CNPase-positive cells in the striatum were 54%, 9%, and 45% and in the cortical tissue were 46%, 7%, and 39%, respectively. Nine percent of the cells in the striatum and 7% of the cells in the cortex coexpressed both NeuN and GFAP markers. The average proportion of NeuN-, GFAP-, and CNPase-positive cells on day 5 of the culture was 21%, 86%, and 41% in the striatum culture and 10%, 64%, and 23% in the cortical tissue culture. The percentage of NeuN, GFAP, CNPase cells in the striatum culture declined to 4%, 36%, and 14% after PTH treatment.

Discussion

The molecular mechanism underlying BGC and the effect of PTH on this calcification is an underexplored area. This study provides new insights into the understanding of BGC

Table 3. mRNA expression of osteogenic molecules in rat striatum and gray matter tissues

SN	Gene	mRNA copies /10^4 copies of housekeeping genes		Difference of copies (striatum to gray)Median IQR	No. tested	*P*
		Striatum	Gray			
Proosteogenic molecules						
1	Osteonectin					
	Mean ± SD	26 460 ± 17 138	15 772 ± 10 148	14 956 (–385 to 18 517)	6	.20
	Median (IQR)	25 667 (12 957-39 267)	14 258 (7196-22 779)			
2	Collagen-1α					
	Mean ± SD	5718 ± 2409	2058 ± 1972	5352 (784 to 5688)	5	.02
	Median (IQR)	6113 (3636-7603)	1874 (553-3657)			
3	*Pit1*					
	Mean ± SD	2400 ± 1110	7688 ± 4075	–4359 (–8217 to –2054)	6	< .01
	Median (IQR)	2524 (1236-3433)	6534 (4409-11 220)			
4	*Pit2*					
	Mean ± SD	755 ± 705	1726 ± 836	–753 (–1844 to –280)	6	.02
	Median (IQR)	564 (254-1113)	1764 (991-2179)			
5	Vitamin D receptor					
	Mean ± SD	3.7 ± 4.8	1.9 ± 2.1	0.2 (0.01 to 5)	6	.13
	Median (IQR)	1.1 (0.6-8.4)	1.1 (0.6-3.2)			
6	Klotho					
	Mean ± SD	101 ± 76	75 ± 54	47 (14 to 3001)	6	.01
	Median (IQR)	85 (41-170)	53 (36-136)			
7	*Bmp2*					
	Mean ± SD	1846 ± 2350	464 ± 301	26 (–312 to 3948)	5	.65
	Median (IQR)	860 (152-3810)	319 (230-770)			
8	Osteocalcin					
	Mean ± SD	82 ± 66	51 ± 42	26 (9 to 60)	6	.01
	Median (IQR)	52 (30-164)	28 (23-101)			
Antiosteogenic molecules						
9	*Ca-II*					
	Mean ± SD	16 589 ± 7769	9525 ± 5074	6202 (1490 to 14 518)	6	.02
	Median (IQR)	19 203 (9869-22 501)	88 825 (5622-11 937)			
10	*Isg15*					
	Mean ± SD	767 ± 640	112 ± 69	470 (262 to 1044)	6	< .001
	Median (IQR)	555 (365-1163)	85 (73-149)			
11	*Pthr2*					
	Mean ± SD	313 ± 269	1116 ± 1217	–456 (–1217 to –117)	6	.08
	Median (IQR)	181 (121-585)	632 (360-1803)			
12	*Enpp1*					
	Mean ± SD	693 ± 382	171 ± 125	448 (124 to 746)	5	< .01
	Median (IQR)	800 (293-1040)	132 (67-278)			
13	Osteopontin					
	Mean ± SD	680 ± 369	351 ± 349	176 (155 to 728)	5	.05
	Median (IQR)	800 (293-1008)	201 (72-713)			
14	*Rank*					
	Mean ± SD	169 ± 49	339 ± 235	–112 (–330 to 8)	6	.09
	Median (IQR)	182 (137-196)	266 (177-492)			
15	Sclerostin					
	Mean ± SD	63 ± 81	45 ± 44	–2 (–11 to 54)	6	.46
	Median (IQR)	18 (4-160)	26 (11-94)			
16	*Darpp32*					
	Mean ± SD	101 000 ± 30 743	9333 ± 6907	91 479 (59 780 to 123 647)	5	.03
	Median (IQR)	106 016 (73 724-125 768)	11 763 (2121-15 332)			

in a hypoparathyroid state using support from autopsy tissues and an ex vivo model. The present study showed that several osteogenic molecules with a procalcification effect were normally expressed in the caudate, dentate, and gray matter along with progenitor cells in humans. With such a large repertoire of procalcification molecules, all 3 brain sites should be susceptible to calcification. Yet, in clinical practice most intracranial calcifications are limited to the basal ganglia (2). The present study assessed the unique pattern of expression of various osteogenic molecules in human caudate tissue and factors that heightened the process of calcification at this site under a hypoparathyroid milieu using an ex vivo model.

Interestingly, 20 molecules were differently expressed in the caudate compared to the gray matter even after stringent correction of significance with the number of molecules tested. The differential expression of several of these molecules would possibly give a positive tilt to the calcification process at the caudate in the presence of triggering stimuli. Thus, high expression of molecules such as *WNT3A*, *FZD4*, β-catenin, and *LRP5* in the caudate tissue would favor calcification through the Wnt3a-canonical pathway of osteogenesis (39). This pathway would be further driven by relatively under-expression of the Dickkopf-1 molecule, which blocks Wnt3a (39). Similarly, the high expression of NT_5E in the caudate nucleus would convert extracellular adenosine 5′-monophosphate (AMP) into "adenosine," which would promote differentiation of mesenchymal stem cells toward osteoblastic lineage through the adenosine$2A_B$ receptor (40). Expression of osteonectin and collagen-1α observed in the caudate region would also facilitate the process of calcification through its calcium-binding action and matrix scaffold formation (41). Strikingly, in gray matter none of the molecules with a procalcification effect had a significantly higher expression than the caudate tissue. The cerebellum dentate nucleus is another area that is prone to calcification, following the basal ganglia region. Interestingly, the expression profile of most of the osteogenic molecules in the dentate nuclei showed a trend similar to that observed at the caudate.

The presence of several molecules with a procalcification effect at the basal ganglia and dentate regions indicated that both regions would have ground susceptible for calcification over cortical gray matter. Moreover, this unique pattern of expression of proosteogenic and antiosteogenic molecules at the caudate and dentate seems to be part of human physiology because the data were based on autopsy tissues of individuals with normal findings. The natural purpose of the expression of osteogenic molecules with a procalcification effect in the caudate region of normal individuals is not known, but could be related to the vital role of these molecules in the structural and functional integrity of the basal ganglia. A recent meta-analysis in humans showed an association of a Wnt-LRP5/6 gene mutation with neurodevelopment defects, attention-deficit/hyperactivity disorder, and cognitive dysfunctions (42). Experimental studies have revealed a significant effect of Wnt3, β-catenin, frizzled receptor, and LRP6 molecules in the maintenance of corticostriatal-glutamatergic synapses and dopaminergic transmission (43). The NT_5E-induced adenosine and its interaction with dopamine are also indispensable for the fine coordination of motor activities mediated through the basal ganglia region (44). Similarly, increased expression of FGFR4 and decreased chordin expression have critical neurotrophic effects on dopaminergic neurons (19, 45).

Interestingly, the present study showed that the caudate nucleus also expressed several molecules with an antiosteogenic action, including osteopontin, *CA-II*, *MGP*, sclerostin, *ISG15*, *ENPP1*, and *USP18* (20, 39, 46). Dense connective tissue or skeletal dysplasia is observed in patients with an inactivating mutation of several of these molecules, including sclerostin, klotho, *MGP*, *ENPP1*, and osteopontin (21, 41, 47-49). The concomitant expression of the several of these antiosteogenic molecules in the caudate could be an evolutionary check to offset the procalcifying effect of Wnt3a, NT_5E, and others while these perform their prodopaminergic actions. The importance of the antiosteogenic role of these molecules in the basal ganglia in normal individuals is supported by the frequent occurrence of BGC in monogenic disorders such as osteopetrosis due to the inactivating mutation of the *CA-II* gene. Bosley et al observed in a series of 18 patients with a *CA-II* mutation a 55% prevalence of BGC at presentation that further increased during follow-up (22). Similarly, patients with a loss of function mutation in genes coding ubiquitin-like proteins, ISG15, or USP18 demonstrate familial BGC (18).

However, most cases of BGC are due to acquired disorders rather than genetic. Postsurgical or idiopathic hypoparathyroidism are the prototype endocrine disorders demonstrating extensive BGC in up to 70% of cases (1, 2). These patients also show progression of BGC during follow-up on conventional vitamin D therapy (2). This study investigated the interplay of various factors leading to BGC in the milieu of chronic hypoparathyroidism using an ex vivo model to explore the possibility of retarding the progression of BGC. The validity of the ex vivo model developed for understanding the process of BGC in humans was indicated by (a) similar expression profile of the osteogenic molecules in the rat striatum, and (b) the presence of absorption peaks characteristic of calcium hydroxyapatite as well as organic matrix and carbonate similar to calvaria cortical bone (50) in calcified nodules in striatal culture as observed in an autopsy of a patient with hypoparathyroidism and BGC (51).

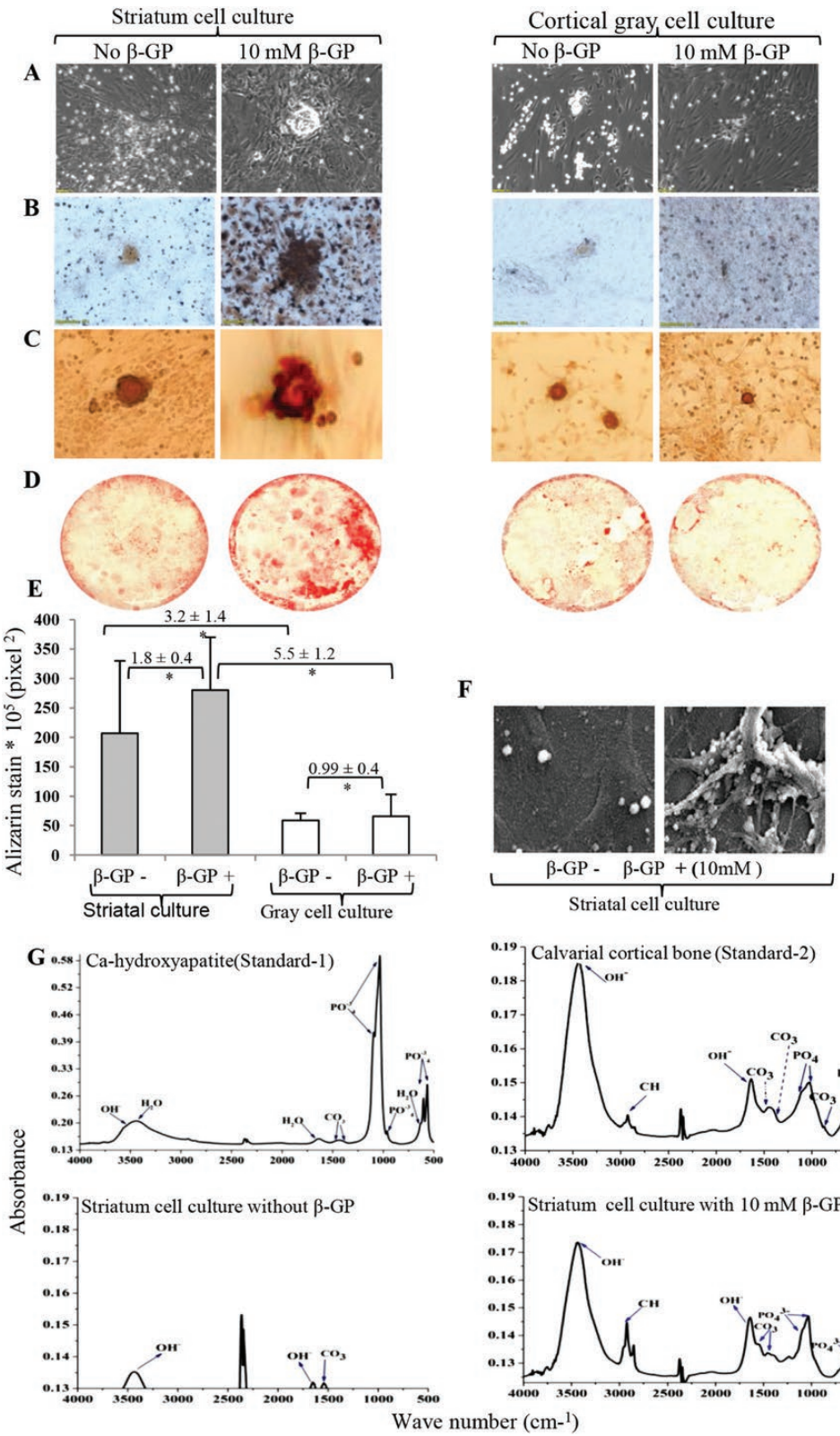

Figure 3. Rat striatum and gray matter culture with and without β-glycerophopshate (β-GP; 10 mM) on the 24th day. A, Phase-contrast microscopy showing distinct nodule in striatum cell culture at 200×. B, Bright-field image of Von-Kossa for phosphorus. C, Alizarin stain for calcium in striatum and gray matter cell culture. D, Stitched image of culture wells showing area under alizarin uptake at 400×. E, Bar diagram showing area under alizarin stain (mean ± SEM) and the fold change (*) in calcification area between striatum vs gray matter culture with and without β-GP. F, Scanning electron microscopy showing mineral deposition on collagen matrix in striatum cell culture with β-GP. G, Fourier-transform infrared spectroscopy spectra of striatal cells cultured in the presence of 10-mM β-GP showing the similarity of the peaks with commercial hydroxyapatite powder and human calvarial cortical bone.

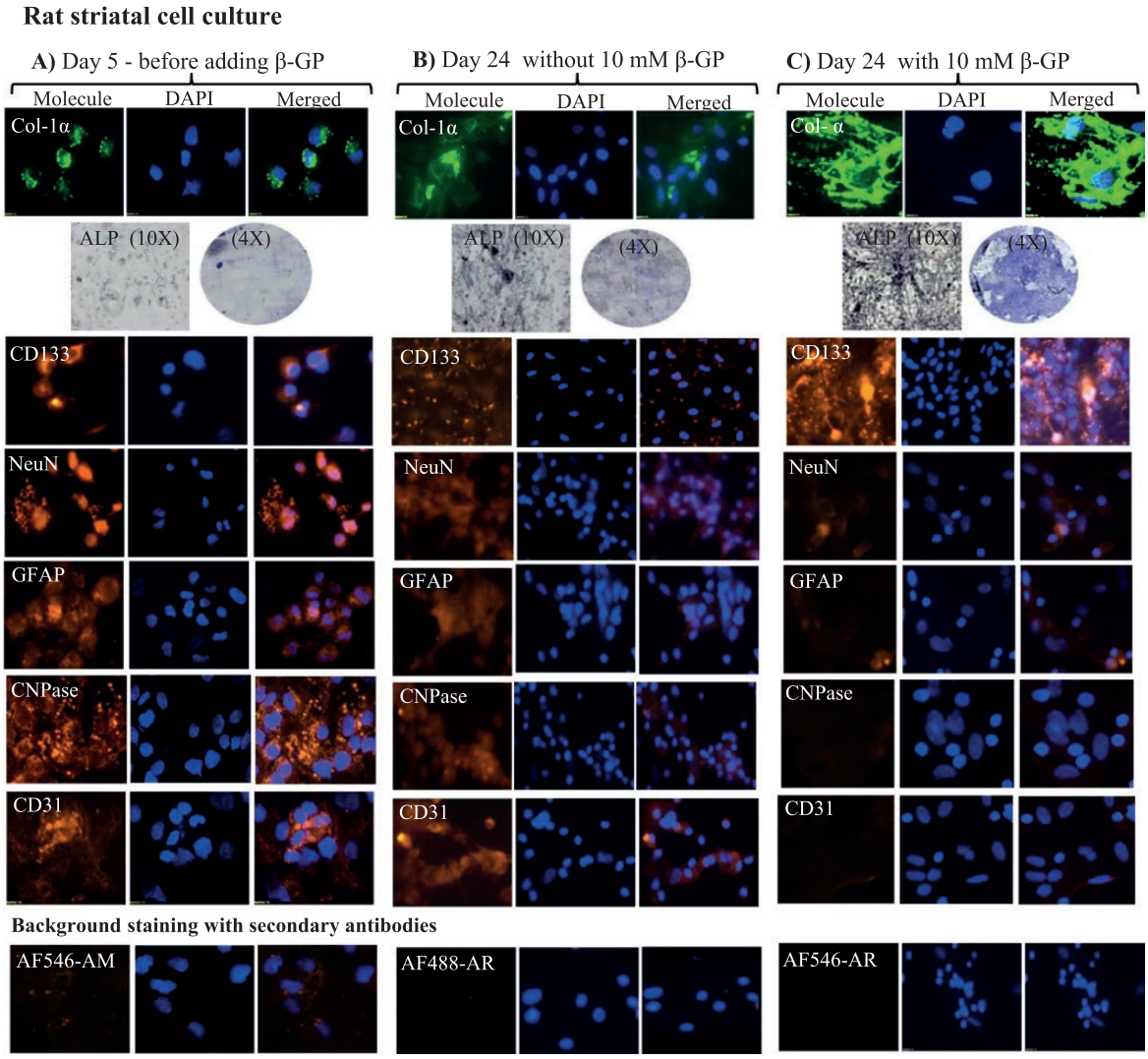

Figure 4. Effect of 10 mM β-glycerophopshate (β-GP) on collagen-1α, alkaline phosphatase, CD133, antineuronal nuclei (NeuN), glial fibrillary acidic protein (GFAP), 2′,3′ cyclic nucleotide 3′- phosphodiesterase (CNPase), and CD31-positive cells in rat striatum culture. A, Epifluorescence microscopy images (600×) for collagen-1α, neuroprogenitor marker CD133, and brain cell markers at baseline, that is, day 5 before adding β-GP along with DAPI (4′,6-diamidino-2-phenylindole; blue) for nuclear localization and their merged image. B,The same molecules stained on day 24 of striatal cell culture with no β-GP added in the media and C, with 10-mM β-GP. Background fluorescence was checked by staining only Alexa Fluor 546 (red) used for brain cell markers, antirabbit–Alexa Fluor 488 (green) used for collagen-1α, and antirabbit Alexa Fluor 546 (red) used for CD133, respectively. Row 2 shows the magnified image of BCIP/NBT stain of the calcified nodule (at 400×) for presence of alkaline phosphatase (ALP). The stitched image of the whole circular coverslip was used for quantifying the area under ALP by cellSens software (Olympus; 40×).

This study revealed that when the cells were cultured in media containing calcium in the hypocalcemic range without any PTH, that is, conditions mimicking the cardinal features of hypoparathyroidism, striatum rather gray-matter cells demonstrated calcifications. This indicated the propensity of the striatal region for calcification. These calcifications increased remarkably by the addition of phosphate salt in the media. This observation provided experimental support to our clinical observation that better phosphatemic control could be relevant to prevent the progression of BGC in hypoparathyroidism (2). Phosphorus-mediated striatal calcification led to a shift in cellular phenotype toward neuro-osteoprogenitor cells as indicated by increased *Cd133*-positive cells, 3-fold higher alkaline phosphatase, and significant collagen-1α secretion. The mismatch between mRNA and protein expression of *Neun*-, *Gfap*-, and *Cnpase*-positive cells on immunofluorescence could be due to posttranslational modifications of these proteins in the presence of procalcification media, which could not be assessed by the antibodies used in this study.

The experiments related to $hPTH_{(1-34)}$ treatment of striatum culture also revealed interesting information of potential clinical relevance. The marked retardation in the size and area of calcified nodules when $hPTH_{(1-34)}$ was added to the striatal cell culture indicated a similar possibility of attenuating BGC during follow-up of patients

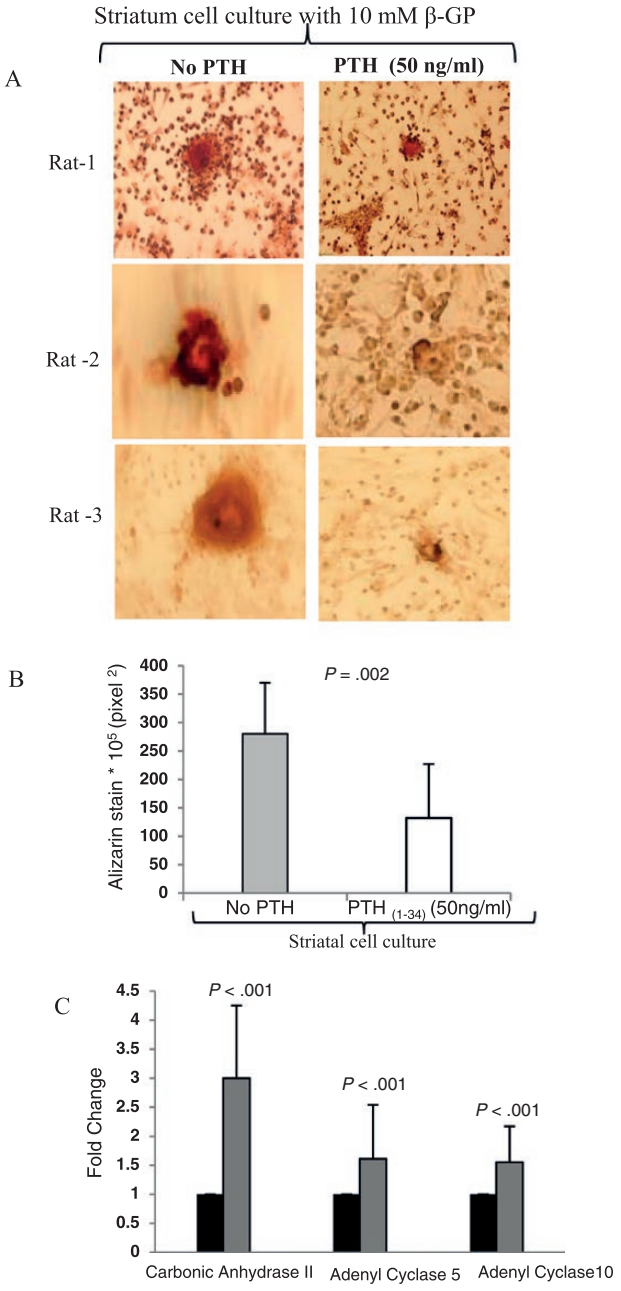

Figure 5. Effect of human recombinant parathyroid hormone ($hPTH_{(1-34)}$) on calcification in rat striatum culture. A, On the 24th day well-defined nodules with intense Alizarin red S stain was observed in striatum cell culture grown in 10 mM of β-glycerophopshate (β-GP) in 3 Sprague-Dawley rats. Smaller-sized nodules and reduced Alizarin stain of these nodules in parathyroid (PTH)-treated media at 50 ng/mL (200×). B, Bar diagram showing the effect of $hPTH_{(1-34)}$ mean area ± SE under Alizarin stain. C, Fold change in messenger RNA expression of carbonic-anhydrase-II, adenyl cyclase (AC)-5, and AC-10 in striatal cell culture after $hPTH_{(1-34)}$ treatment for 10 days. Gray bars indicate culture with $hPTH_{(1-34)}$ and black bars indicate culture without $hPTH_{(1-34)}$.

with hypoparathyroidism with the use of upcoming PTH therapy. There is no previous experimental or clinical report on the effect of $hPTH_{(1-34)}$ on the attenuation of calcification in the basal ganglia region and its effector molecules. The present study showed the attenuation of calcification with $hPTH_{(1-34)}$ was associated with increased expression of type 5 and 10 isoforms of adenyl-cyclase, *Ca-II*, and *Usp18* and decreased expression of *Nt5e*, which together would favor activation of antiosteogenic activity in striatal cells. Interestingly, Smits et al in 1983 reported an increase in cerebral adenyl-cyclase–mediated 3′,5′-cyclic AMP (cAMP) level in cerebrospinal fluid following injection of 200 IU of bovine PTH in 3 healthy volunteers (52). The increase in adenyl-cyclase 5 observed following the addition of $hPTH_{(1-34)}$ in the striatal culture could consequently enhance cellular cAMP and CA-II expression through the cAMP response element on this gene (53).

To the best of our knowledge, this is the first ex vivo model of BGC using rat striatum tissue. This simple model not only helped enhance clarity on the mechanism of BGC in hypoparathyroidism but also provides useful information in relation to other diseases. As an example, this model can also be used to understand the interconnection of various osteogenic molecules with dopamine pathways in the striatum and their possible relevance in relation to Parkinson disease.

The limitations of the present study include a lack of information on the biochemical parameters of the autopsies and nonavailability of basal ganglia tissues from hypoparathyroid individuals in view of rarity of the disease. The model developed for BGC is simple, potent, inexpensive, and possible to replicate under routine laboratory conditions. However, it would require a correction in the future. For example, the current model of striatum cell calcification would help the study of the effect of PTH, though its cellular components might not reflect the in vivo condition. The proportions of glial cells adherent to poly-D-lysine–coated culture wells were 3-folds higher, unlike the in vivo condition, in which neuronal cells are the predominant cells in the striatum as well as the cortex tissue (54). The loss of neuronal and glial markers following PTH treatment under in vitro culture also needs to be assessed in the in vivo condition. Further, the present study used 10 mM of β-GP to obtain a clear picture on the effect of high phosphate on intracranial calcification in the striatum and gray matter and its underlying mechanisms during a short period of culture. Hypoparathyroidism is a chronic condition, and BGC develops over a period of several years of follow-up on calcium and vitamin D therapy. In the preliminary stages of standardization of an ex vivo model, use of 2 mM of β-GP elicited only a moderate degree of calcification in the striatal culture. Further studies assessing the effect of β-GP ranging from 2 to 10 mmol for a longer duration of culture along with modulation of the vitamin D content of the culture media would further fine-tune

Table 4. Effect of parathyroid hormone treatment on messenger RNA expression of osteogenic molecules in rat striatum cell culture (N = 6)

SN	Molecule	mRNA copies/10^4 copies of housekeeping genes		*P*
		Control (no PTH)	Treated (with PTH)	
Proosteogenic molecules				
1	β-Catenin1			
	Mean ± SD	5321 ± 1977	5265 ± 1333	.35
	Median (IQR)	4496 (4029-7095)	5418 (4278-5711)	
2	Osteonectin			
	Mean ± SD	273 928 ± 70 076	239 572 ± 81 824	.43
	Median (IQR)	290 968 (227 107-330 860)	240 727 (156 938-321 369)	
3	Klotho			
	Mean ± SD	25 ± 13	21 ± 7	.81
	Median (IQR)	21 (18-26)	21 (15-27)	
4	*Fzd4*			
	Mean ± SD	409 ± 224	405 ± 257	.99
	Median (IQR)	298 (258–550)	330 (273–487)	
5	*NT_5E*			
	Mean ± SD	7094.9 ± 1668.5	5843.9 ± 1739.7	.02
	Median (IQR)	7023.3 (6036.2-8003.9)	6059.5 (4404.2-7030.0)	
6	*Lrp5*			
	Mean ± SD	118 ± 35	121 ± 35	.81
	Median (IQR)	116 (90-135)	124 (94-141)	
7	Collagen-1α			
	Mean ± SD	120 137 ± 42 312	96 828 ± 36 634	.53
	Median (IQR)	118 262 (77 119-152 272)	82 711 (73 276-105 942)	
8	*Wnt5a*			
	Mean ± SD	805.5 ± 283.7	1193.8 ± 636.4	.02
	Median (IQR)	844.3 (665.2-995.0)	1139.7 (819.8-1555.5)	
9	*Fzd9*			
	Mean ± SD	327.8 ± 169.3	265.4 ± 154.4	.46
	Median (IQR)	281.2 (196.1-463.0)	275.6 (166.0-312.6)	
10	*Msx-2*			
	Mean ± SD	6236.7 ± 2582.3	9188.8 ± 3949.3	.06
	Median (IQR)	5654.7 (4688.3-7022.9)	8696.7 (5989.1-11 685.7)	
11	Osteoprotegerin			
	Mean ± SD	5975.8 ± 2545.3	7401.6 ± 3836.6	.30
	Median (IQR)	5159.4 (4430.1-7986.3)	6987.7 (4670.1-8541.1)	
12	*Fgfr1*			
	Mean ± SD	3716.8 ± 998.1	5542.0 ± 2671.4	.04
	Median (IQR)	3600.6 (3139.7-4504.1)	5113.8 (3995.5-6344.0)	
13	*Fgfr4*			
	Mean ± SD	5.7 ± 3.0	4.3 ± 1.4	.31
	Median (IQR)	5.4 (2.5-8.1)	4.6 (2.8-5.4)	
14	*Pit1*			
	Mean ± SD	3504 ± 1192	2921 ± 824	.99
	Median (IQR)	3402 (2388-4482)	2696 (2303-3551)	
15	*Pit2*			
	Mean ± SD	1327.2 ± 373.3	1535.9 ± 1629.1	.68
	Median (IQR)	1174.7 (1109.0-1547.9)	1083.3 (876.8-1474.1)	
Antiosteogenic molecules				
16	Osteopontin			
	Mean ± SD	43 047 ± 22 050	34 358 ± 15 548	.53
	Median (IQR)	35 769 (26 036-53 176)	30 224 (20 628-49 586)	
17[a]	*Ca-II*			
	Mean ± SD	453 ± 350	1315 ± 958	< .001
	Median (IQR)	365 (234-523)	1106 (763-1729)	
18	*Mgp*			
	Mean ± SD	9467 ± 3577	7348 ± 1939	.13
	Median (IQR)	8940 (7321-10 700)	7266 (5531-9368)	

Table 4. Continued

SN	Molecule	mRNA copies/10^4 copies of housekeeping genes		*P*
		Control (no PTH)	Treated (with PTH)	
19	Sclerostin			
	Mean ± SD	129 ± 78	147 ± 80	.16
	Median (IQR)	113 (72–193)	128 (101-172)	
20	*Isg15*			
	Mean ± SD	464 ± 186	466 ± 306	.99
	Median (IQR)	410 (323-659)	387 (301-442)	
21	*Enpp1*			
	Mean ± SD	3911 ± 1232	3084 ± 911	.58
	Median (IQR)	4184 (2846–4673)	3200 (2172-3873)	
22	*Usp18*			
	Mean ± SD	5089.8 ± 3040.7	7551.1 ± 3663.5	.04
	Median (IQR)	5346.5 (2873.9–6931.5)	6257.8 (5555.8-9163.5)	
23	Chordin			
	Mean ± SD	177 ± 70	162 ± 74	.81
	Median (IQR)	165 (123-206)	138 (97-237)	
24	*Rank*			
	Mean ± SD	84 ± 29	75 ± 30	.95
	Median (IQR)	86 (55-100)	70 (46-97)	
25	Dickkopf1			
	Mean ± SD	1515.8 ± 496.3	2079.0 ± 1362.9	.28
	Median (IQR)	1504.2 (1172.1-1962.3)	1649.0 (1090.2-2367.5)	
26	*Pthr2*			
	Mean ± SD	15 496.2 ± 8344.1	10 573.0 ± 6263.2	.22
	Median (IQR)	12 066.4 (9502.0-21 892.5)	10 194.7 (6311.9-13 431.6)	
27	*Xpr1*			
	Mean ± SD	1907.2 ± 553.5	1488.2 ± 656.0	.08
	Median (IQR)	1781.3 (1626.4-2072.3)	1617.0 (1178.1-2054.2)	
28	*Pcdh12*			
	Mean ± SD	483.0 ± 261.6	615.7 ± 353.1	.27
	Median (IQR)	380.4 (258.9-766.2)	662.7 (343.7-821.3)	
29	*Pdgf*			
	Mean ± SD	6690.1 ± 2347.0	9325.0 ± 5913.9	.27
	Median (IQR)	5889.6 (4721.1-9238.9)	7726.5 (5652.3-10 416.6)	
30	*Pthr1*			
	Mean ± SD	1070 ± 598	860 ± 323	.94
	Median (IQR)	852 (614-1334)	768 (581-1117)	
Adenyl cyclases				
31[a]	Adenyl cyclase 5			
	Mean ± SD	821 ± 438	1683 ± 1074	< .001
	Median (IQR)	697 (570-1031)	1428 (977-1857)	
32[a]	Adenyl cyclase 10			
	Mean ± SD	89 ± 39	188 ± 140	< .001
	Median (IQR)	76 (59-116)	131 (105-197)	
33	Adenyl cyclase 3			
	Mean ± SD	573 ± 189	587 ± 257	.79
	Median (IQR)	558 (385-814)	582 (392-657)	
34	Adenyl cyclase 2			
	Mean ± SD	49 ± 20	37 ± 20	.09
	Median (IQR)	47 (38-55)	27 (22-54)	
35	Adenyl cyclase 9			
	Mean ± SD	115 ± 41	95 ± 41	.29
	Median (IQR)	103 (84-155)	82 (71-103)	

[a]*Ca-II*, adenyl cyclase 5, and adenyl cyclase 10 were assessed in 13 rats.

this model nearer to the internal milieu of patients with hypoparathyroidism.

Thus, the present study provides novel information relevant to the clinical problem of BGC in patients with hypoparathyroidism through an ex vivo experimental model of BGC. Fig. 6 shows a schematic representation of the unique environment of the caudate nuclei and its heightened susceptibility to calcification in hypoparathyroid milieu based on information obtained from the autopsy tissue and the ex vivo model. With high expression of Wnt-catenin and NT_5E molecules in most neurons, astrocytes, and endothelial cells along with the presence of neuroprogenitor cells, the caudate region can be considered constitutively predisposed to calcification. However, calcification at the caudate region would be triggered when it is exposed to further hits such as (a) increased phosphate levels and/or (b) subnormal PTH. Hyperphosphatemia and subnormal PTH are cardinal biochemical features of hypoparathyroidism. The ex vivo model showed that both these cardinal features can synergistically enhance striatal calcification through separate routes. High phosphate in the presence of the Wnt-pathway and neural-progenitor cells enriched the environment of the caudate and would promote osteogenic differentiation. On the other hand, subnormal PTH would downregulate antiosteogenic molecules, foremost being CA-II. Interestingly, increased CA-II expression following exogenous $hPTH_{(1\text{-}34)}$ and attenuated striatum calcification provides hope of a similar phenomenon in patients with hypoparathyroidism and BGC. Clinical studies using PTH therapy in patients with primary hypoparathyroidism with

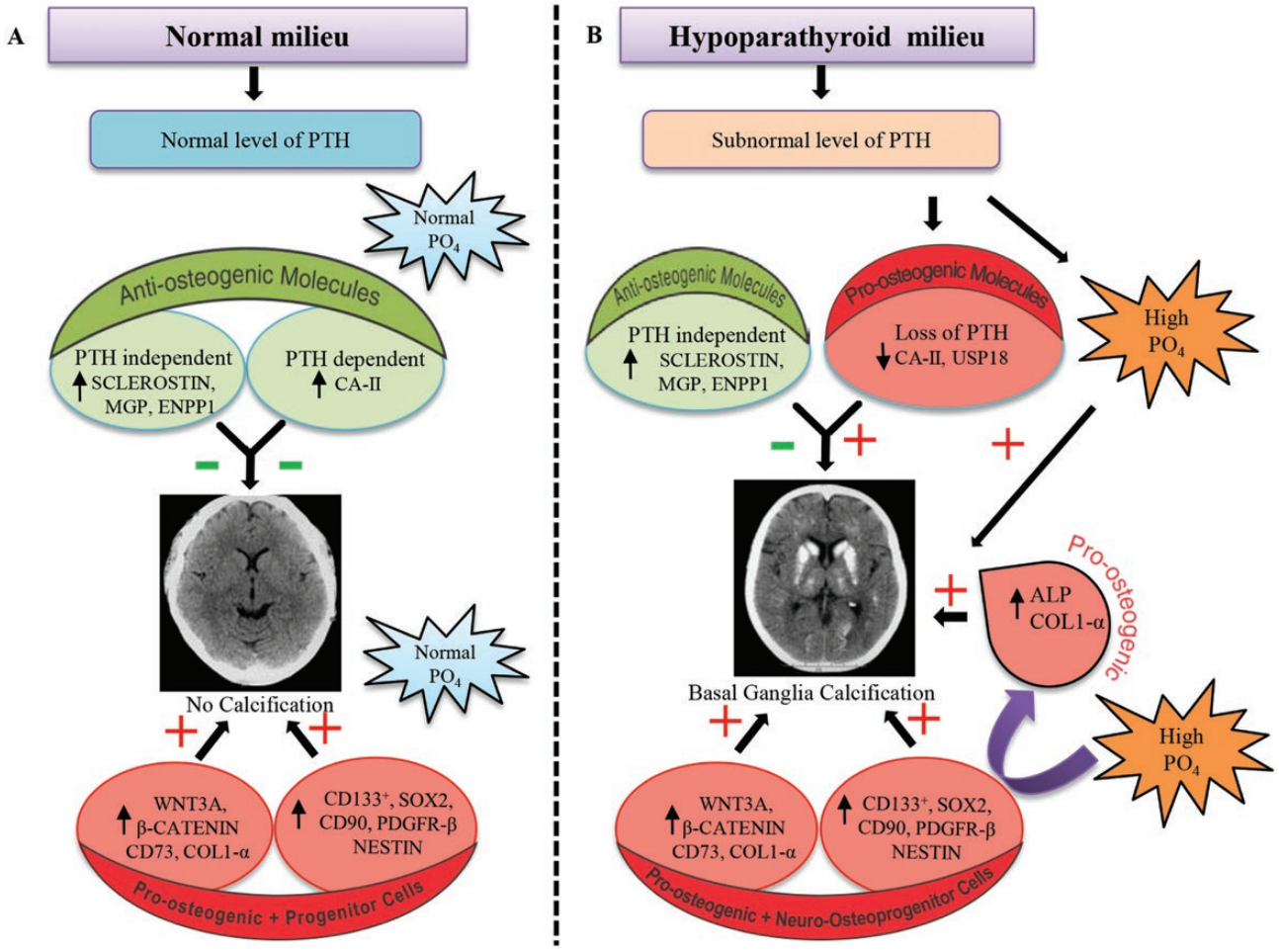

Figure 6. Schematic illustration of possible roles of proosteogenic and antiosteogenic factors in basal ganglia calcification. A, In a normal, healthy state, there is a concomitant expression of proosteogenic and antiosteogenic molecules in the basal ganglia region. In the presence of normal phosphate and parathyroid hormone (PTH), these molecules do not trigger the process of calcification. B, In the hypoparathyroid state, subnormal PTH leads to high circulating phosphate and decreased expression of carbonic anhydrase-II (CA-II). High phosphate can independently induce a shift toward neuro-osteoprogenitor cells, leading to increased secretion of collagen-1α and alkaline phosphatase (ALP). The decreased expression of CA-II in the caudate tissue and the consequent loss of its calcium resorptive action would tilt the balance of osteogenic molecules to a procalcification state, leading to basal ganglia calcification.

an objective to assess reduction in the prevalence or progression of BGC would further help provide the translation effect of the present work.

Acknowledgments

The authors thank the Advanced Instrumentation Research Facility, Jawaharlal Nehru University, New Delhi, for confocal images; the University Science Instrumentation Centre, University of Delhi, for FTIR spectroscopy; and the Central Research Facility, Indian Institute of Technology, New Delhi, for scanning electron microscopy. The authors acknowledge the Central Animal Facility of the All India Institute of Medical Sciences, New Delhi, for providing Sprague-Dawley rats. The authors also acknowledge the help of doctoral committee members of P.K., namely, Prof N. Tandon and Prof V.P. Jyostna (Department of Endocrinology), Prof T.S. Roy (Department of Anatomy), Prof P.P. Chattopadhyay (Department of Biochemistry), Prof R. Tandon (Department of Ophthalmology), and Prof V. Sreenivas (Department of Biostatistics) for their advice during the study.

Financial Support: This work was supported by the All India Institute of Medical Sciences, New Delhi (intramural grant No. A-252), the Indian Council of Medical Research, New Delhi, India (3/1/2/39/2014-15 (Nut. 2016-2019 for fellowship of Ms Parmita Kar), and Department of Biotechnology, Department of Science and Technology, India (BT/PR22675/MED/30/1806/2016, 2019 to the present).

Author Contributions: The study was designed by R.G., P.K., and S.S.. T.M. helped in obtaining all the autopsy tissues. P.K. carried out all the experiments. S.S. contributed to the experiments related to real-time PCR and development of the ex vivo model. S.M. helped with the experiments related to the ex vivo model. S.A. helped with assessment of colocalization of various osteogenic molecules in different brain cells. R.G., S.S., and P.K. contributed the analyzing the data. All the authors contributed to the writing of the manuscript.

Additional Information

Correspondence: Ravinder Goswami, MD, DM (Endocrinology), Department of Endocrinology and Metabolism, All India Institute of Medical Sciences, Biotechnology Block Ansari Nagar, Rm No. 304, New Delhi 110029, Delhi, India (gosravinder@hotmail.com).

Disclosures: The authors have nothing to disclose.

Data Availability: All data generated or analyzed during this study are included in this published article or in the data repositories listed in "References." (https://doi.org/10.6084/m9.figshare.13516457.v2)

References

1. Gafni RI, Collins MT. Hypoparathyroidism. *N Engl J Med*. 2019;**380**(18):1738-1747.
2. Goswami R, Sharma R, Sreenivas V, Gupta N, Ganapathy A, Das S. Prevalence and progression of basal ganglia calcification and its pathogenic mechanism in patients with idiopathic hypoparathyroidism. *Clin Endocrinol (Oxf)*. 2012;**77**(2):200-206.
3. Aggarwal S, Kailash S, Sagar R, et al. Neuropsychological dysfunction in idiopathic hypoparathyroidism and its relationship with intracranial calcification and serum total calcium. *Eur J Endocrinol*. 2013;**168**(6):895-903.
4. Goswami R, Millo T, Mishra S, et al. Expression of osteogenic molecules in the caudate nucleus and gray matter and their potential relevance for basal ganglia calcification in hypoparathyroidism. *J Clin Endocrinol Metab*. 2014;**99**(5):1741-1748.
5. Hofbauer LC, Brueck CC, Shanahan CM, Schoppet M, Dobnig H. Vascular calcification and osteoporosis–from clinical observation towards molecular understanding. *Osteoporos Int*. 2007;**18**(3):251-259.
6. Nicolas G, Sanchez-Contreras M, Ramos EM, et al. Brain calcifications and PCDH12 variants. *Neurol Genet*. 2017;**3**(4):e166.
7. Huang L, Xu J, Wood DJ, Zheng MH. Gene expression of osteoprotegerin ligand, osteoprotegerin, and receptor activator of NF-κB in giant cell tumor of bone: possible involvement in tumor cell-induced osteoclast-like cell formation. *Am J Pathol*. 2000;**156**(3):761-767.
8. Zhai Y, Chen L, Hömme M, et al. Expression and function of matrix Gla protein in human peritoneal mesothelial cells. *Nephrol Dial Transplant*. 2010;**25**(10):3213-3221.
9. Osyczka AM, Diefenderfer DL, Bhargave G, Leboy PS. Different effects of BMP-2 on marrow stromal cells from human and rat bone. *Cells Tissues Organs*. 2004;**176**(1-3):109-119.
10. Diefenderfer DL, Osyczka AM, Garino JP, Leboy PS. Regulation of BMP-induced transcription in cultured human bone marrow stromal cells. *J Bone Joint Surg Am*. 2003;**85-A**(Suppl 3):19-28.
11. Witkowski JM, Soroczyńska-Cybula M, Bryl E, Smoleńska Z, Jóźwik A. Klotho—a common link in physiological and rheumatoid arthritis-related aging of human $CD4^+$ lymphocytes. *J Immunol*. 2007;**178**(2):771-777.
12. Kirikoshi H, Sekihara H, Katoh M. Expression profiles of 10 members of Frizzled gene family in human gastric cancer. *Int J Oncol*. 2001;**19**(4):767-771.
13. van Bezooijen RL, Roelen BA, Visser A, et al. Sclerostin is an osteocyte-expressed negative regulator of bone formation, but not a classical BMP antagonist. *J Exp Med*. 2004;**199**(6):805-814.
14. Forget MA, Turcotte S, Beauseigle D, et al. The Wnt pathway regulator DKK1 is preferentially expressed in hormone-resistant breast tumours and in some common cancer types. *Br J Cancer*. 2007;**96**(4):646-653.
15. Schwartz PH, Bryant PJ, Fuja TJ, Su H, O'Dowd DK, Klassen H. Isolation and characterization of neural progenitor cells from post-mortem human cortex. *J Neurosci Res*. 2003;**74**(6):838-851.
16. Smyth LCD, Rustenhoven J, Scotter EL, et al. Markers for human brain pericytes and smooth muscle cells. *J Chem Neuroanat*. 2018;**92**:48-60.
17. Guo XX, Zou XH, Wang C, et al. Spectrum of *SLC20A2*, *PDGFRB*, *PDGFB*, and *XPR1* mutations in a large cohort of patients with primary familial brain calcification. *Hum Mutat*. 2019;**40**(4):392-403.
18. Meuwissen ME, Schot R, Buta S, et al. Human USP18 deficiency underlies type 1 interferonopathy leading to severe pseudo-TORCH syndrome. *J Exp Med*. 2016;**213**(7):1163-1174.
19. Gratsch TE, O'Shea KS. Noggin and chordin have distinct activities in promoting lineage commitment of mouse embryonic stem (ES) cells. *Dev Biol*. 2002;**245**(1):83-94.

20. Wang C, Xu X, Li LL, et al. Molecular mechanism of idiopathic basal ganglia calcification [article in Chinese]. *Yi Chuan*. 2015;**37**(8):731-740.
21. Oheim R, Zimmerman K, Maulding ND, et al. Human heterozygous ENPP1 deficiency is associated with early onset osteoporosis, a phenotype recapitulated in a mouse model of Enpp1 deficiency. *J Bone Miner Res*. 2020;**35**(3):528-539.
22. Bosley TM, Salih MA, Alorainy IA, et al. The neurology of carbonic anhydrase type II deficiency syndrome. *Brain*. 2011;**134**(Pt 12):3502-3515.
23. Kar P, Millo T, Saha S, Mahtab S, Agarwal S, Goswami R. Osteogenic mechanisms of basal ganglia calcification and its ex-vivo model in hypoparathyroid milieu. *figshare*. Dataset. January 15, 2021; https://doi.org/10.6084/m9.figshare.13516457.v2
24. Stan AD, Ghose S, Gao XM, et al. Human postmortem tissue: what quality markers matter? *Brain Res*. 2006;**1123**(1):1-11.
25. Goswami R, Mohapatra T, Gupta N, et al. Parathyroid hormone gene polymorphism and sporadic idiopathic hypoparathyroidism. *J Clin Endocrinol Metab*. 2004;**89**(10):4840-4845.
26. Kar P, Chawla H, Saha S, Tandon N, Goswami R. Identification of reference housekeeping-genes for mRNA expression studies in patients with type 1 diabetes. *Mol Cell Biochem*. 2016;**417**(1-2):49-56.
27. Goswami R, Brown EM, Kochupillai N, et al. Prevalence of calcium sensing receptor autoantibodies in patients with sporadic idiopathic hypoparathyroidism. *Eur J Endocrinol*. 2004;**150**(1):9-18.
28. Pereira S, Veeraraghavan P, Ghosh S, Gandhi M. Animal experimentation and ethics in India: the CPCSEA makes a difference. *Altern Lab Anim*. 2004;**32**(Suppl 1B):411-415.
29. Spijker S. Dissection of rodent brain regions. In: Li K, ed. *Neuroproteomics*. *Neuromethods*. **Vol. 57**. Humana Press; 2011.
30. Bonefeld BE, Elfving B, Wegener G. Reference genes for normalization: a study of rat brain tissue. *Synapse*. 2008;**62**(4):302-309.
31. Langenbach F, Handschel J. Effects of dexamethasone, ascorbic acid and β-glycerophosphate on the osteogenic differentiation of stem cells in vitro. *Stem Cell Res Ther*. 2013;**4**(5):117.
32. Lee K, Kwon M, Jeong D. In vitro biomineralization assay. *Bio Protoc*. 2014;**4**(3):e1036.
33. Louvet L, Bazin D, Büchel J, Steppan S, Passlick-Deetjen J, Massy ZA. Characterisation of calcium phosphate crystals on calcified human aortic vascular smooth muscle cells and potential role of magnesium. *PloS One*. 2015;**10**(1):e0115342.
34. Lee Y, Messing A, Su M, Brenner M. GFAP promoter elements required for region-specific and astrocyte-specific expression. *Glia*. 2008;**56**(5):481-493.
35. Matsuoka I, Suzuki Y, Defer N, Nakanishi H, Hanoune J. Differential expression of type I, II, and V adenylyl cyclase gene in the postnatal developing rat brain. *J Neurochem*. 1997;**68**(2):498-506.
36. Strazzabosco M, Fiorotto R, Melero S, et al. Differentially expressed adenylyl cyclase isoforms mediate secretory functions in cholangiocyte subpopulation. *Hepatology*. 2009;**50**(1):244-252.
37. Bek MJ, Zheng S, Xu J, et al. Differential expression of adenylyl cyclases in the rat nephron. *Kidney Int*. 2001;**60**(3):890-899.
38. Rubio FJ, Li X, Liu QR, Cimbro R, Hope BT. Fluorescence activated cell sorting (FACS) and gene expression analysis of Fos-expressing neurons from fresh and frozen rat brain tissue. *J Vis Exp*. 2016;(114):e54358.
39. Hampson G, Edwards S, Conroy S, Blake GM, Fogelman I, Frost ML. The relationship between inhibitors of the Wnt signalling pathway (Dickkopf-1(DKK1) and sclerostin), bone mineral density, vascular calcification and arterial stiffness in post-menopausal women. *Bone*. 2013;**56**(1):42-47.
40. Takedachi M, Oohara H, Smith BJ, et al. CD73-generated adenosine promotes osteoblast differentiation. *J Cell Physiol*. 2012;**227**(6):2622-2631.
41. Sakamoto A, Oda Y, Iwamoto Y, Tsuneyoshi M. A comparative study of fibrous dysplasia and osteofibrous dysplasia with regard to expressions of *c-fos* and *c-jun* products and bone matrix proteins: a clinicopathologic review and immunohistochemical study of *c-fos*, *c-jun*, type I collagen, osteonectin, osteopontin, and osteocalcin. *Hum Pathol*. 1999;**30**(12):1418-1426.
42. Grünblatt E, Nemoda Z, Werling AM, et al. The involvement of the canonical Wnt-signaling receptor *LRP5* and *LRP6* gene variants with ADHD and sexual dimorphism: association study and meta-analysis. *Am J Med Genet B Neuropsychiatr Genet*. 2019;**180**(6):365-376.
43. Jia L, Piña-Crespo J, Li Y. Restoring Wnt/β-catenin signaling is a promising therapeutic strategy for Alzheimer's disease. *Mol Brain*. 2019;**12**(1):104.
44. Augusto E, Matos M, Sévigny J, et al. Ecto-5′-nucleotidase (CD73)-mediated formation of adenosine is critical for the striatal adenosine A2A receptor functions. *J Neurosci*. 2013;**33**(28):11390-11399.
45. Claus P, Werner S, Timmer M, Grothe C. Expression of the fibroblast growth factor-2 isoforms and the FGF receptor 1-4 transcripts in the rat model system of Parkinson's disease. *Neurosci Lett*. 2004;**360**(3):117-120.
46. Jahnen-Dechent W, Schäfer C, Ketteler M, McKee MD. Mineral chaperones: a role for fetuin-A and osteopontin in the inhibition and regression of pathologic calcification. *J Mol Med (Berl)*. 2008;**86**(4):379-389.
47. Loots GG, Kneissel M, Keller H, et al. Genomic deletion of a long-range bone enhancer misregulates sclerostin in van Buchem disease. *Genome Res*. 2005;**15**(7):928-935.
48. Razzaque MS. The FGF23-Klotho axis: endocrine regulation of phosphate homeostasis. *Nat Rev Endocrinol*. 2009;**5**(11):611-619.
49. Superti-Furga A, Bonafé L, Rimoin DL. Molecular-pathogenetic classification of genetic disorders of the skeleton. *Am J Med Genet*. 2001;**106**(4):282-293.
50. Addison WN, Nelea V, Chicatun F, et al. Extracellular matrix mineralization in murine MC3T3-E1 osteoblast cultures: an ultrastructural, compositional and comparative analysis with mouse bone. *Bone*. 2015;**71**:244-256.
51. Muenter MD, Whisnant JP. Basal ganglia calcification, hypoparathyroidism, and extrapyramidal motor manifestations. *Neurology*. 1968;**18**(11):1075-1083.
52. Smits MG, Gabreëls FJ, Froeling PG, de Abreu RA, Thijssen HO, Renier WO. Calcium-phosphate metabolism in autosomal recessive idiopathic strio-pallido-dentate calcinosis and Cockayne's syndrome. *Clin Neurol Neurosurg*. 1983;**85**(3):145-153.
53. Marino LR. Characterization of the mouse carbonic anhydrase II gene promoter. *J Biol Chem*. 1993;**268**(10):7081-7089.
54. Keller D, Erö C, Markram H. Cell densities in the mouse brain: a systematic review. *Front Neuroanat*. 2018;**12**:83.